

Research Articles | Cellular/Molecular

The intellectual disability risk gene Kdm5b regulates long term memory consolidation in the hippocampus

<https://doi.org/10.1523/JNEUROSCI.1544-23.2024>

Received: 18 February 2024

Revised: 21 March 2024

Accepted: 30 March 2024

Copyright © 2024 Perez-Sisques et al.

This is an open-access article distributed under the terms of the [Creative Commons Attribution 4.0 International license](#), which permits unrestricted use, distribution and reproduction in any medium provided that the original work is properly attributed.

This Early Release article has been peer reviewed and accepted, but has not been through the composition and copyediting processes. The final version may differ slightly in style or formatting and will contain links to any extended data.

Alerts: Sign up at www.jneurosci.org/alerts to receive customized email alerts when the fully formatted version of this article is published.

1
2 **The intellectual disability risk gene *Kdm5b* regulates long term**
3 **memory consolidation in the hippocampus**
4
5
6

7 Leticia Perez-Sisques^{1,2}, Shail Bhatt¹, Rugile Matuleviciute², Talia Gileadi¹, Eniko
8 Kramar³, Andrew Graham¹, Franklin G. Garcia³, Ashley Keiser³, Dina P. Matheos³,
9 James A. Cain¹, Alan M. Pittman⁴, Laura C. Andrae², Cathy Fernandes^{2,5}, Marcelo
10 A. Wood³, K. Peter Giese⁶ and M. Albert Basson^{1,2,7}

11 ¹ Centre for Craniofacial and Regenerative Biology, Guy's Hospital, King's College London, London
12 SE1 9RT, UK

13 ² MRC Centre for Neurodevelopmental Disorders, Institute of Psychiatry, Psychology and
14 Neuroscience, King's College London, New Hunt's House, London SE1 1UL, UK

15 ³ Department of Neurobiology and Behavior, School of Biological Sciences, University of California
16 Irvine, Irvine, CA, USA

17 ⁴ St. George's University of London, Cranmer Terrace, London SW17 0RE, UK

18 ⁵ Social, Genetic & Developmental Psychiatry Centre, Institute of Psychiatry, Psychology and
19 Neuroscience, King's College London, 16 De Crespigny Park, London SE5 8AB, UK

20 ⁶ Department of Basic and Clinical Neuroscience, Institute of Psychiatry, Psychology and
21 Neuroscience, King's College London, Maurice Wohl Clinical Neuroscience Institute, 5 Cutcombe Rd,
22 London SE5 9RT, UK

23 ⁷ Department of Clinical and Biomedical Sciences, Faculty of Health and Life Sciences, Hatherley
24 Laboratories, Prince of Wales Road, University of Exeter Medical School, University of Exeter, Exeter,
25 EX4 4PS, UK
26
27
28
29
30
31
32

33 Correspondence:

34
35 Prof. M. Albert Basson
36 Department of Clinical and Biomedical Sciences
37 University of Exeter Medical School
38 Hatherley Laboratories
39 Prince of Wales Road
40 Exeter
41 EX4 4PS
42 UK
43
44
45

46 The authors have declared that no conflict of interest exists.
47
48
49
50
51

52 Keywords: KDM5B, histone lysine demethylase, hippocampus, learning, memory, mouse,
53 chromatin
54

58 **Abstract**

59

60 The histone lysine demethylase KDM5B is implicated in recessive intellectual disability
61 disorders and heterozygous, protein truncating variants in *KDM5B* are associated with
62 reduced cognitive function in the population. The KDM5 family of lysine demethylases has
63 developmental and homeostatic functions in the brain, some of which appear to be
64 independent of lysine demethylase activity. To determine the functions of KDM5B in
65 hippocampus-dependent learning and memory, we first studied male and female mice
66 homozygous for a *Kdm5b*^{ΔARID} allele that lacks demethylase activity. *Kdm5b*^{ΔARID/ΔARID} mice
67 exhibited hyperactivity and long-term memory deficits in hippocampus-dependent learning
68 tasks. The expression of immediate early, activity-dependent genes was downregulated in
69 these mice and hyperactivated upon learning stimulus compared to wildtype mice. A number
70 of other learning-associated genes was also significantly dysregulated in the
71 *Kdm5b*^{ΔARID/ΔARID} hippocampus. Next, we knocked down *Kdm5b* specifically in the adult,
72 wildtype mouse hippocampus with shRNA. *Kdm5b* knockdown resulted in spontaneous
73 seizures, hyperactivity and hippocampus-dependent long-term memory and long-term
74 potentiation deficits. These findings identify KDM5B as a critical regulator of gene expression
75 and synaptic plasticity in the adult hippocampus and suggest that at least some of the
76 cognitive phenotypes associated with *KDM5B* gene variants are caused by direct effects on
77 memory consolidation mechanisms.

78

79 **Significance statement**

80 The histone lysine demethylase KDM5B has been implicated in cognitive performance and
81 intellectual disability conditions in the human population. In the present manuscript we show
82 that mice expressing a demethylase-deficient KDM5B and mice with a specific knockdown of
83 KDM5B in the adult hippocampus exhibit hippocampus-dependent learning and memory
84 phenotypes. Molecular analyses suggest a key role for KDM5B in regulating the dynamic
85 expression of activity-regulated genes during memory consolidation. Deficits in LTP are
86 present in mice with KDM5B knockdown. Together, these findings provide the first evidence
87 for a direct function for KDM5B in memory consolidation in the hippocampus.

88

89

JNeurosci Accepted Manuscript

90 Introduction

91 Genome sequencing studies have implicated genes encoding chromatin modifying factors in
92 intellectual disability and autism spectrum disorders (ID and ASD). These include the gene
93 *KDM5B* (Lysine demethylase 5B), recessive mutations of which are linked to a rare ID
94 syndrome (Faundes et al., 2018; Martin et al., 2018). Intriguingly, *KDM5B* is tolerant to loss-
95 of-function mutations, and a significant proportion of such heterozygous *KDM5B* variants are
96 incompletely penetrant and inherited (Wang et al., 2022; Zhou et al., 2022). A recent study
97 reported that rare protein truncating variants in *KDM5B* are associated with large effects on
98 cognitive function in the population (Chen et al., 2023). Specifically, protein truncating
99 variants in *KDM5B* negatively correlated with educational attainment, reaction time and
100 verbal-numerical reasoning. This study also reported an association of protein truncating
101 variants of *KDM5B* with neurodevelopmental and psychiatric disorders and epilepsy. The
102 same study found initial evidence that a heterozygous and homozygous deletion of *Kdm5b*
103 exon 7 in mice was associated with dose-dependent cognitive deficits and increased anxiety
104 (Chen et al., 2023). Previous studies have reported significant embryonic or perinatal
105 lethality of homozygous *Kdm5b* loss-of-function mutations in mice. The deletion of exon 1
106 was associated with lethality by embryonic day 7.5 (Catchpole et al., 2011), whereas either
107 exon 6 (Albert et al., 2013) or exon 7 (Martin et al., 2018) deletion was associated with 36-
108 44% postnatal viability, suggesting that the deletion of exons 6 or 7 produces hypomorphic
109 alleles with partially penetrant effects.

110

111 *KDM5B*, together with *KDM5A* and *KDM5C*, are the only histone lysine demethylases known
112 to demethylate trimethylated lysine 4 on histone 3 (H3K4me3), a post-translational histone
113 modification typically present at active gene promoters. H3K4me3 can recruit components of
114 transcriptional initiator (Vermeulen and Timmers, 2010; Lauberth et al., 2013), and integrator
115 complexes (Wang et al., 2023). The latter is associated with the regulation of transcriptional
116 output by stimulating transcriptional elongation (Wang et al., 2023). As *KDM5B* specifically

117 removes H3K4me3 to counteract this process, the lack of KDM5B demethylase activity is
118 predicted to lead to transcriptional de-repression of direct target genes. H3K4me3 is also
119 enriched at non-methylated CpG island promoters, where it is thought to counteract DNA
120 methylation (Hughes et al., 2020).

121

122 The *KDM5A-D* genes in mammals are paralogues of the ancestral *KDM5* gene in
123 *Drosophila*. *KDM5* mutation is also associated with lethality (Gildea et al., 2000). *Drosophila*
124 *KDM5* can regulate gene expression with multiple mechanisms, including a mechanism that
125 requires the PHD domain of the protein, and appear to function independently from the
126 demethylase activity of the protein (Liu and Secombe, 2015). Indeed, *Drosophila* *KDM5* and
127 mammalian *KDM5* proteins interact with other chromatin factors and complexes that function
128 as transcriptional repressors, including components of Sin3/HDAC1 and NuRD complexes
129 (Yheskel et al., 2023). Thus, some *KDM5B*-mediated transcriptional repression may be
130 mediated by demethylase-independent mechanisms. Flies with mutations in the
131 demethylase domains of the protein survive, consistent with demethylase-independent
132 functions, but exhibit specific learning phenotypes (Zamurrad et al., 2018; Belalcazar et al.,
133 2021).

134

135 Mutations in the lysine methyltransferases responsible for H3K4me3, KMT2A and KMT2B
136 are also associated with autosomal dominant ID syndromes (Jones et al., 2012; Faundes et
137 al., 2018). Animal experiments have shown that a learning stimulus results in a rapid and
138 transient increase in H3K4me3 levels in the hippocampus, similar to immediate early gene
139 induction (Gupta et al., 2010). Consistent with a functional role for H3K4me3, the lysine
140 methyltransferases, KMT2A and KMT2B are necessary for normal hippocampus-dependent
141 learning and memory in mice (Kerimoglu et al., 2013; Kerimoglu et al., 2017).

142

143 Together, these studies suggest that dysregulation of H3K4me3, either by loss of function of
144 methyltransferases or demethylases, can result in ID. Conditional deletion of *Kmt2a* and
145 *Kmt2b* genes in post-mitotic neurons in the mouse, was sufficient to cause learning and
146 memory phenotypes, suggesting that defects in the H3K4me3 machinery directly impacts
147 memory consolidation mechanisms in the hippocampus (Kerimoglu et al., 2013; Kerimoglu
148 et al., 2017). Thus, to understand how KDM5B loss-of-function affects learning and memory,
149 we set out to determine if KDM5B has a direct function in memory consolidation, as opposed
150 to having exclusively developmental functions. We focused on the hippocampus as the
151 function of this brain region in learning and memory is well-established, and hippocampus-
152 dependent memory tasks and electrophysiological correlates such as long-term potentiation
153 (LTP) are robust in mice.

154

155

156

157 **Materials and Methods**

158

159 **Animals**

160 Experiments with mice carrying the *Kdm5b*^{tm1.Jtpu}, referred to as the *Kdm5b*^{ΔARID} allele
161 (Catchpole et al., 2011) were performed at King's College London. *Kdm5b*^{ΔARID/ΔARID} males
162 on a C57BL/6J background were crossed with 129S2/Sv females to produce heterozygous
163 F1 mice, that were then inter-crossed to produce WT and homozygous *Kdm5b*^{Δ/Δ} F2 mice for
164 experiments. Experimental cohorts of mice were derived from 5 (studies with naïve mice) to
165 15 (for behavioural analyses) litters. Animals were housed in ventilated cages (37x20x16cm)
166 with *ad libitum* access to water and food (Labdiet Picolab rodent irradiated diet, #5R53) and
167 kept at 19–22°C and 40–60% humidity, under a 12:12-h light/dark cycle. The cages
168 contained bedding (Lignocel wood fiber) and nesting. A maximum of five animals were
169 housed in the same cage. All animal procedures were approved by the King's College
170 London AWERB and the UK Home Office.

171 **Genotyping of mice**

172 Genotyping was performed by extracting genomic DNA from ear notches as previously
173 described (Hurley et al., 2021). The following primer pairs to detect the WT and the mutant
174 alleles were used: WT forward 5'- CCTTAGACGCAGACAGCACA-3', WT reverse 5'-
175 CGTGTTTGGGCCTAAATGTC-3', *Kdm5b*-ΔARID forward 5'-
176 TGCTCCTGCCGAGAAAGTATCC-3' and *Kdm5b*-ΔARID reverse 5'-
177 CCACCCCCCAGAATAGAATGA-3'. Thermal cycles for the genotyping reactions were as
178 follows: 95°C, 2 min; 35x (95°C, 15 sec; 64°C, 15 sec; 72°C, 15 sec); 72°C, 12min.

179 ***Kdm5b* knock-down**

180 Adult (8-12 week old) female C57BL/6J mice received 1 μl (1x10¹⁰ viral particles) of either
181 AAV1-CMV-GFP-U6-m*Kdm5b*-shRNA, Vector Biolabs #shAAV-262769) or control AAV1-
182 CMV-GFP-U6-scrambled shRNA, #7040) in both dorsal hippocampi as described (Kwapis et

183 al., 2018). These experiments were approved by the UCI IACUC and KCL AWERB and UK
184 Home office.

185 **Western blot**

186 Brain cortices were dissected from adult mice and whole cell protein prepared by lysing in
187 8M urea, 1% CHAPS, 50mM Tris (pH 7.9) lysis buffer containing protease inhibitors.
188 Samples were rotated for 30 min at 4°C and then centrifuged for 50 min to remove DNA.
189 Supernatant was stored at -80°C. All reagents and machinery were obtained from BioRad
190 unless stated otherwise. Samples were prepared with Laemmli buffer containing 10% β -
191 mercaptoethanol and resolved with 7.5% Mini-PROTEAN pre-cast polyacrylamide gels and
192 Tris/Glycine/SDS buffer. 60 μ g of protein were prepared to detect KDM5B protein in brain
193 lysates. Proteins were transferred to a nitrocellulose membrane with the TransBlot turbo
194 system (High molecular weight transfer program). Membranes were blocked with 5% BSA
195 (Sigma) diluted in tris-buffered saline containing 0.1% Tween-20 (TBS-T). Primary
196 antibodies were diluted in TBS-T containing 5% BSA. Primary antibodies were incubated
197 overnight at 4°C in 5% BSA in TBS-T. Membranes were incubated with secondary
198 antibodies diluted in TBS-T containing 5% BSA for 1h at room temperature. Proteins were
199 detected with Clarity ECL reagent and membranes were imaged using the Chemidoc
200 system. Densitometric analyses were performed with ImageJ software (NIH). The following
201 antibodies were used: anti-KDM5B (Abcam, ab181089, 1:1000), α Tubulin (Upstate, 05-829),
202 goat anti-rabbit and anti-mouse HRP secondary antibodies (Thermo Fisher Scientific,
203 #31460 and Proteintech, #SA00001-1, respectively, 1:5000). Uncropped full scans of the
204 blots shown in Figure 1B are shown in Extended Data Figure 1-1.

205 **Immunofluorescence**

206 Animals were perfused with either 1x PBS or 1x PBS followed by 4% paraformaldehyde
207 (PFA). Brains were removed and fixed overnight in 4% PFA. Samples were cryopreserved
208 with a sucrose gradient (5%, 15%, 30%, one day each). Free-floating coronal brain sections

209 (20-30 μ m) were obtained with a cryostat. Sections were first washed twice in PBS-T (1x
210 PBS 0.3% Triton X-100) and blocked for 1h in blocking buffer (BB: PBS-T 3% NGS 3%
211 BSA). Following blocking, primary antibodies were incubated overnight in BB at 4°C. The
212 following day, slices were washed twice with PBS-T and secondary antibodies were
213 incubated in BB for 2h. Samples were washed three times with PBS-T before nuclei staining
214 with Hoechst3332 (1:5000). Two final washes with 1x PBS were performed before mounting
215 with anti-fade mounting media (Abcam, ab104135). The following antibodies were used
216 (1:200 dilution): Npas4 (Activity signaling, NP41-2), GFP (Abcam, ab13970), H3K4me3 (Cell
217 Signaling Technologies, 9751S), goat anti-rabbit 488 (Thermo Fisher Scientific, A11031),
218 and goat anti-chicken 488 (Thermo Fisher Scientific, A11039. Images were acquired with a
219 Zeiss Axio Observer7 microscope (20x magnification) and Zen Blue software. Image
220 acquisition and analysis were performed blindly. The number of Npas4-positive nuclei in the
221 hippocampal layers CA3 and DG was quantified manually with the Cell Counter plug-in on
222 ImageJ-FIFI (NIH). The number/density and mean staining intensity/cell of H3K4me3 were
223 analysed in CA1/2, CA3 and dentate gyrus with QuPath (Bankhead et al., 2017). The
224 following settings were used to detect the positive cells: Requested pixel size: 0.5;
225 Background radius: 8; Median filter radius: 0; Sigma: 1.5; Cell expansion: 2 (all in μ m);
226 Minimum area: 10; Maximum area: 400 (in μ m²); Threshold: 10.

227 **Golgi staining and spine analysis**

228 Fresh brain hemispheres were processed with the FD Rapid GolgiStain™ kit (FD
229 Neurotechnologies) following manufacturer's instructions. Briefly, 100 μ m sections were
230 obtained with a vibratome and mounted on gelatine-coated superfrost slides. Following the
231 staining procedure, brightfield images of impregnated dendrites from dorsal hippocampal
232 neurons were captured with a Zeiss Axio Observer7 microscope (63x magnification) and Zen
233 Blue software. Stacks were taken every 0.2 μ m and analysed manually with FIJI. Spine
234 density was calculated in 10 proximal dendrites per area and animal, starting 5 μ m apart
235 from the ramification. Spine density values are shown as average for each area and animal.

236 **Behaviour**

237 Different cohorts of control and *Kdm5b*-mutant mice were used for the experiments in this
238 study: 1) battery of behavioural tests (Fig. 3), 2) confirmation of the anxiety-related
239 phenotype, 3) RNAseq with naïve animals (Fig. 4A,B), 4) confirmation of the RNAseq results
240 by immunofluorescence and RT-qPCR (Fig. 4C-E), and 5) RNAseq to study gene
241 expression changes upon learning (Fig. 5). For the *Kdm5b* knock-down experiment (Fig. 6),
242 a cohort of mice was used for the behavioural and the electrophysiology analyses, and extra
243 cohorts were used to confirm the *Kdm5b* knock-down one, three, and seven weeks after the
244 surgery. A final cohort was dedicated to study the effect of the knock-down on early gene
245 expression 11 days after the surgery.

246 Behavioural assessments of F2 mice (cohort 1) started at 7-8 weeks of age, consisting of the
247 following: handling, open field test, object location memory test, elevated plus maze,
248 spontaneous alternation in a Y-maze test, Morris water maze, fear conditioning test and
249 measurement of grip strength. Mice were left to rest for at least 2 days in between tests.
250 Mice in cohorts 3, 4 and 5 were 7-8 weeks old when samples were collected.

251 Behavioural experiments were conducted between 8:00 and 18:30 under standard room
252 lighting conditions unless stated otherwise. Cages were changed every two weeks but never
253 less than 48h before the day of testing. Behaviours were tracked using Ethovision (Noldus
254 Information Technologies bv, Wageningen, The Netherlands). After each trial of a specific
255 test, boli and urine were removed, and the test area was cleaned with 1% Anistel® (high
256 level surface disinfectant, Trisel Solution Ltd, Cambridgeshire, UK, for cohort 2) or 10%
257 ethanol (cohort 1) to remove any odours. The experiments were blinded and randomized by
258 blocks of mice. Littermates were used as controls with multiple litters examined per
259 experiment (15 for cohort 1 and 12 for cohort 2). Mice were habituated to the behavioural
260 room conditions for at least 30 minutes before the start of each testing session. Before the
261 start of the experiments, mice were individually handled for 5 consecutive days, 2 minutes
262 each day.

263 Behavioural assessments of shRNA mice were started 2-3 weeks after stereotactic
264 surgeries. Mice were first tested in the elevated plus maze to determine effects on activity
265 and anxiety, handled for 5 days as described and habituated to the test arena for 6 days
266 before training with two identical objects for 10 minutes, followed by a 5 min test session 24h
267 later with one of the objects moved to a new location (Kwapis et al., 2018). Two weeks later,
268 tissue was collected for acute slice preparations and LTP.

269 *Open field*

270 The circular open field arena was made of clear acrylic with a grey base, with internal
271 dimensions of 40 cm diameter and 40 cm high as described (Whittaker et al., 2017). Light
272 intensity inside the arena was 10 lux. Two virtual areas were drawn on Ethovision: a centre
273 zone, 20cm diameter, and a ring 5 cm thick around the perimeter of the arena was defined
274 as the outer zone. Test mice were placed in the open field facing an outer wall to begin the
275 test. Its locomotor activity was tracked for 5 minutes. Total distance moved (cm) in the outer
276 zone was used as a measure of the level of locomotive activity and time (s) spent in the
277 centre zone used as a measure of anxiety.

278 *Object location memory test*

279 The test was performed as described in (Vogel-Ciernia et al., 2013). The arena (40x40x40
280 cm) was made of white acrylic and had a black stripe in one of the walls as an internal cue.
281 Light intensity was 40 lux in the centre of the arena. Briefly, mice were habituated to the
282 arena for 6 consecutive days, 5 minutes/day. During the training session, mice were placed
283 for 10 minutes in the arena with the two identical objects (100 ml glass beakers filled with
284 cement to prevent them being moved by the mice) next to the wall with the visual cue. 24 h
285 later, during the test session, one of the two objects was randomly moved to the opposite
286 side of the arena, in a centre position, and mice were left to explore the arena for 5 minutes.
287 Exploration was manually scored and the following criteria was used: nose of the mouse is
288 within 1cm of the object, with their head directly facing it. Rearing, standing on the object,

289 and digging near it were not considered as exploratory behaviours. Discrimination index (DI)
290 was calculated as: (time exploring new location – time exploring old location) / (total
291 exploration time) * 100. Exclusion criteria included exploration time below 3 seconds for
292 either training or testing sessions, and DI above +/-20 for the training session.

293 *Elevated plus maze (EPM)*

294 The EPM was made of black acrylic and consisted of four arms (30 x 5 cm). The two
295 opposing closed arms were enclosed by 15 cm high walls on each side and ends. The two
296 opposing open arms were open, as well as the centre platform (5 x 5 cm). The maze was
297 elevated 40 cm above ground. Light intensity was 100 lux on the open arms and 10 lux on
298 the closed arms. The number of entries onto, time spent on, and latency to enter the closed
299 and open arms were manually scored. An arm entry is defined when all 4 paws were located
300 inside the arm. Mice were placed in the centre platform of the EPM facing a closed arm to
301 start the 5 minutes test.

302 *Spontaneous alternation in a Y-maze*

303 The Y maze apparatus was made of grey acrylic and consisted of three arms, 120° from
304 each other. All arms were 45cm long, 5 cm wide and enclosed by a 10cm wall. Extramaze
305 visual cues were placed at the end of each arm. One arm was considered as the central
306 arm, and the other two arms were randomly closed during the training session. During the
307 training session, mice were placed in the maze in the central arm and allowed to explore it
308 for 10 minutes, after which they were returned to their homecage. After 1h, the testing
309 session was conducted. Both arms were open, and mice were placed in the central arm and
310 allowed to freely explore the maze for 5 minutes. The first choice to turn either to the familiar
311 arm or the new arm (percentage of alternation rate) was monitored, when all four paws were
312 inside that arm. Arm preference was automatically monitored with Ethovision and the
313 Discrimination index was calculated as (time exploring new arm – time exploring old arm) /
314 (total exploration time of the old and new arms) * 100.

315 *Morris water maze*

316 Spatial learning and memory were assessed using a Morris water maze (MWM). The maze
317 (1 m diameter) was filled with water, made opaque with a non-toxic white aqueous emulsion.
318 Water temperature was 23°C, and light intensity was 100lux. A set of extra-maze visual cues
319 were suspended around the pool. Four alternative start positions were nominated to provide
320 the virtual division of the tank into four quadrants. Mice were trained to find a hidden platform
321 (10 cm diameter), submerged 2 cm below the water surface, for 8 consecutive days, four
322 trials a day. Once they found the platform, mice were left on it for 15 seconds before
323 returning them to their homecage. Mice that failed to locate the hidden platform after 60
324 seconds were placed on the platform for 15 seconds. Animals that failed to stay on the
325 platform following two days of training were excluded from the study. On probe trial the
326 platform was removed and mice were placed into the pool for 60 seconds so they could
327 freely explore the tank. To check for deficiencies in vision or locomotion, mice were placed in
328 the pool with a visible platform (1cm above the surface, with a flag attached to it), one day,
329 four trials. Mouse movement was tracked with Ethovision to calculate mean speed, total
330 distance travelled in the pool and in each quadrant, and the number of platform crossings
331 during the probe trial.

332 *Fear conditioning test*

333 Animals were placed in a soundproof fear conditioning apparatus with stainless steel metal
334 grid floor, containing a camera (Med Associates Inc.). To provide an olfactory cue, an
335 ethanol-soaked tissue was placed under the grid in both training and testing sessions.
336 Mouse behaviour was recorded with VideoFreeze software. For conditioning, mice were
337 placed inside the chamber and left to freely explore it. After 148 seconds, three electric
338 shocks (0.7mA, 2 sec each, 30 seconds apart) were administered. The animals were then
339 removed from the testing chamber after 30 additional seconds. 24 h later, mice were placed
340 in the same chamber for 5 minutes. Freezing behaviour was manually scored from recorded

341 videos during training and testing sessions. Freezing behaviour was defined as the complete
342 lack of movement during the first 2 seconds of each 5-second window.

343 *Grip strength measurements*

344 To assess the neuromuscular ability of the animals, fore- and hindlimb grip strength was
345 measured with a Linton Grip Strength Meter (MJS Technology, Ltd). Mice were pulled across
346 the meter from left to right measuring forelimb and then hindlimb strength. The average of
347 three measurements per limb and mouse was taken.

348 **RNA extraction**

349 Total RNA was extracted from hippocampal samples with 1ml TRIzol (Thermo Fisher
350 Scientific) and further purified with the Monarch Total RNA miniprep kit (New England
351 Biolabs) following the manufacturer's recommendations (including DNase treatment step).

352 **qRT-PCR analysis**

353 cDNA was synthesised from 200-400ng RNA with UltraScript 2.0 cDNA Synthesis kit (PCR
354 Biosystems) according to the manufacturer's instructions. qRT-PCRs were performed on a
355 BioRad CFX384 using qPCRBIO SyGreen Mix Lo-ROX (PCR Biosystems). Relative
356 expression levels were calculated using the $2^{-\Delta\Delta CT}$ method and *Hprt* or *Gapdh* were used as
357 endogenous control genes. For shRNA experiments, the PrimeTime probe-based gene
358 expression system (IDT) was used to quantify *Kdm5b* expression, relative to *Hprt*. Primer
359 sequences: *Arc* (Fw: 5'-CTCAACTTCCGGGGATGCAG-3', Rv: 5'-
360 CTGGTATGAATCACTGGGGGC-3'), *cFos* (Fw: 5'-AGAGCGGGAATGGTGAAGAC-3', Rv:
361 5'-AGTTGATCTGTCTCCGCTTGG-3'), *Egr1* (Fw: 5'-TGAGCACCTGACCACAGAGTC-3',
362 Rv: 5'-TAACTCGTCTCCACCATCGC-3'), *Egr2* (Fw:5'-GTGCTGCCTGACAGCCTCTA-3',
363 Rv: 5'-TTGATCATGCCATCTCCCGCC-3'), *Gapdh* (Fw: 5'-AGGTCGGTGTAACGGATTTG-
364 3', Rv: 5'-TGTAGACCATGTAGTTGAGGTCA-3'), *Hprt* (Fw: 5'-
365 GTCCCAGCGTCGTGATTAGC-3', Rv: 5'-TGGCCTCCCATCTCCTTCAT-3'), *Kdm5b* (Fw:
366 5'-AAGCCAAGCTCTGTTCAGCAA-3', Rv: 5'-GAAGGCAATCGTTCTTCTCACT-3'), *Npas4*

367 (Fw: 5'-CTGCATCTACTCGCAAGG-3', Rv: 5'-GCCACAATGTCTTCAAGCTCT-3'),
368 Kdm5b (for Fig. 6, Fw: 5'-CAAGAGCCCACTGAGAAGAAA-3', Rv: 5'-
369 TCCACATAAGAGGCACACATAC-3') and Hprt (for Fig. 6, Fw: 5'-
370 TGCTCGAGATGTCATGAAGG-3', Rv: 5'-CTTTTATGTCCCCCGTTGAC-3').

371 **RNAseq**

372 Total RNA (n=4/genotype, balanced for sex) were sent to Novogene for library preparation
373 and sequencing. After mRNA enrichment, mRNA quality was analysed using Agilent Total
374 RNA 6000 Pico on a Bioanalyser (Agilent, 2100). Pair-end sequencing (150bp read length)
375 was performed on the Illumina Novaseq 6000 platform. Further data analyses were
376 performed using the Galaxy Europe server (<https://usegalaxy.eu>)
377 (<https://academic.oup.com/nar/article/50/W1/W345/6572001>). Quality of the raw data was
378 checked using FastQC (v0.11.9). Reads were aligned to the mouse genome (mm10) using
379 RNA STAR (v2.7.8a), and aligned reads were counted using FeatureCounts (v2.0.1).
380 Differential expression analyses were performed using DESeq2 (v2.11.40.7). Multiple
381 comparisons were controlled for using an FDR < 0.05. Exact p values and adjusted p-values
382 for all differentially expressed genes are listed in Extended data Table 4-1 and Table 5-1.
383 Genes with adjusted p-value <0.05 were considered as differentially expressed genes
384 (DEGs). Heatmaps were generated with the R package pheatmap. Volcano plots were
385 generated in GraphPad Prism 9.4.1. Differentially expressed genes in at least one
386 comparison (any timepoint between genotypes, or 1h/0h, 3h/0h and 3h/1h within the same
387 genotype) were clusterised with k-means clustering and selecting the optimal cluster number
388 for the dataset (k=4). Activity-induced genes were obtained from (Chen et al., 2017), with
389 only differentially upregulated transcripts detected by both RNAseq and TRAPseq included.
390 Gene ontology analyses were conducted using g:Profiler (<https://biit.cs.ut.ee/gprofiler/gost>),
391 where GO molecular function and GO biological process of size 0-1500 were checked. The
392 applied threshold was "Benjamini Hochberg FDR < 0.05".

393

394 **Electrophysiology**

395 Female mice (n=4/treatment, 8 total) were sacrificed for electrophysiology and hippocampal
396 slices prepared as described previously (Vogel-Ciernia et al., 2013). Mice were
397 anesthetized, decapitated, and the brains rapidly removed into ice-cold, oxygenated
398 dissection medium containing (in mM): 124 NaCl, 3 KCl, 1.25 KH₂PO₄, 5 MgSO₄, 0 CaCl₂,
399 26 NaHCO₃, and 10 glucose. Hippocampal slices (320 μm, coronal) were cut from a
400 vibratome (Leica, Model:VT1000S) before transferred to an interface recording containing
401 prewarmed (31 ± 1° C) artificial cerebrospinal fluid (aCSF) composed of (in mM): 124 NaCl,
402 3 KCl, 1.25 KH₂PO₄, 1.5 MgSO₄, 2.5 CaCl₂, 26 NaHCO₃, and 10 glucose. Slices were
403 perfused continuously at a rate of 1.75-2 ml/min while the surface of the slices were exposed
404 to warm, humidified 95% O₂/5% CO₂. Recordings began following at least 2h of incubation.

405 Field excitatory postsynaptic potentials (fEPSPs) were recorded from CA1b stratum radiatum
406 apical dendrites using a glass pipette filled with 2M NaCl (2-3 MΩ) in response to
407 orthodromic stimulation (twisted nichrome wire, 65 μm diameter) of Schaffer collateral-
408 commissural projections in CA1c stratum radiatum. Pulses were administered 0.05 Hz using
409 a current that elicited a 50% maximal spike-free response. After maintaining a stable
410 baseline (20 min), long-term potentiation (LTP) was induced by delivering 5 'theta' bursts,
411 with each burst consisting of four pulses at 100 Hz separated by 200 msec (i.e., theta burst
412 stimulation or TBS). The stimulation intensity was not increased during TBS. Data were
413 collected and digitized by NAC 3.0 (Neurodata Acquisition System, Theta Burst Corp., Irvine,
414 CA) and stored on a disk.

415 Data in the text are presented as means ± SD, while in the figures as mean ± SEM. The
416 fEPSP slope was measured at 10–90% fall of the slope and data in figures on LTP were
417 normalized to the last 20 min of baseline.

418 **Statistics**

419 Data are reported as mean \pm SEM. Graphs show individual data points. Normal distribution
420 was tested with d'Agostino and Pearson omnibus, Shapiro-Wilk and Kolmogorov-Smirnov
421 normality tests. If the test was passed, statistical analysis was performed using parametric
422 statistical analyses. Before pairs of comparisons, we performed the F test to compare
423 variances. In experiments with normal distribution statistical analyses were performed using
424 the unpaired two-sided Student's t test. T-test with Welch's correction was applied when
425 variances were unequal. Two- and Three-way ANOVA with the appropriate post hoc tests
426 were also performed as indicated in the figure legends. Significant p values ($p < 0.05$) are
427 reported in the results section and/or figure legends provide details of relevant statistical
428 parameters, including group sizes. Statistical analyses were performed with GraphPad Prism
429 (version 9.4.1). Experiments in this study were blinded and animals randomised for in vivo
430 studies.

431

432 **Results**

433 **KDM5B demethylase-deficient mice exhibit megalencephaly**

434 *Kdm5b* ^{Δ ARID/ Δ ARID} (*Kdm5b* ^{Δ/Δ}) mice were generated to circumvent the embryonic and early
435 postnatal lethality of other loss-of-function models. The deletion of exons 2 to 4 leads to a
436 partial truncation of the JmjN domain and the deletion of the ARID domain of the KDM5B
437 protein (Fig. 1A), that disrupts its H3K4me3 demethylase activity (Jamshidi et al., 2021). We
438 confirmed the loss of full-length KDM5B protein and the appearance of a shorter KDM5B-
439 Δ ARID protein in the brain of adult *Kdm5b* ^{Δ/Δ} mice by Western blot (Fig. 1B,C). The mutant
440 KDM5B- Δ ARID protein appears to be either unstable or not as well detected by KDM5B-
441 specific antiserum in western blot, leading to an apparent reduction in total KDM5B protein
442 levels in the homozygous mutants, compared to wildtype mice (Fig. 1D). We did not observe
443 differences between male and female animals.

444 To assess the impact on H3K4me3, hippocampal sections from *Kdm5b*^{Δ/Δ} and control mice
445 were immunostained with an antibody to H3K4me3. We observed a clear increase in the
446 number of H3K4me3-positive cells in the hippocampus (Fig. 1E,F). This increase was
447 observed in both sexes (Two-way ANOVA sex effect: $F_{1,4}=0.1824$, $p=0.6913$). Moreover, the
448 intensity of H3K4me3 across the population of cells in the hippocampus shifted towards
449 increased H3K4me3 in the mutants in all hippocampal subregions, cornu ammonis 1 (CA1)
450 (Fig. 1G,H), cornu ammonis 3 (CA3) (Fig. 1I,J) and dentate gyrus (DG) (Fig. 1K,L).

451 In an attempt to further reduce any developmental abnormalities associated with KDM5B
452 deficiency, all animals used in this study were on a C57BL/6Jx129S2/Sv F2 genetic
453 background (Zou et al., 2014, and data from the International Mouse phenotyping
454 Consortium (IMPC): <http://www.mousephenotype.org/>). Homozygous *Kdm5b*^{Δ/Δ} mice
455 generated on this genetic background generated from heterozygous intercrosses were
456 present at expected ratios at P21 (Fig. 2A). Postnatal *Kdm5b*^{Δ/Δ} mice displayed a growth
457 deficit and reduced body weights (Fig. 2B). Homozygous mutants exhibited increased brain-
458 to-body weight ratios at postnatal day 21, while the liver-to-body weight ratios did not differ
459 between genotypes, suggesting specific neurodevelopmental alterations (Fig. 2C-G).
460 Histological assessments did not reveal any gross abnormalities in cortical architecture (Fig.
461 2H,I) or spine density in proximal dendrites of CA1) pyramidal neurons and of DG granule
462 cells in the hippocampus (Fig. 2J).

463

464 **Hippocampus-dependent learning and memory deficits in *Kdm5b*^{Δ/Δ} mice**

465 To determine whether KDM5B loss of function affects learning and memory, we tested these
466 mice in hippocampus-dependent tasks. Data from males and females were combined,
467 unless mice of different sexes exhibited differences in specific tests, where the data from
468 both sexes are shown. During the handling sessions we observed that the reduced body
469 weight observed at pre-weaning stages was still evident at 2 months of age (Fig. 3A).

470 *Kdm5b^{ΔΔ}* mice exhibited hyperactivity in the open field (Fig. 3B). They also spent less time in
471 the inner area of the arena, suggesting an anxiety-like phenotype (Fig. 3C). However, this
472 phenotype was not observed in the elevated plus maze (EPM) in the same cohort of mice
473 (Fig. 3D) and was not consistent in a second cohort (for that cohort: distance travelled in the
474 open field genotype effect: $p=0.9966$; time (%) spent in the open arms in the EPM genotype
475 effect: $*p=0.0385$), suggesting that the anxiety-like phenotype is variable and potentially
476 secondary to hyperactivity. Next, we performed the novel object location memory test (OLM)
477 to study long-term spatial memory. A significant deficit in long-term spatial memory was
478 observed in the mutant mice 24 h after training (Fig. 3E). Exploration times were equal
479 between genotypes in both training and testing sessions (Fig. 3F), indicating a specific deficit
480 in object location memory. In contrast, short term spatial memory and cognitive flexibility was
481 preserved in *Kdm5b^{ΔΔ}* mice, as judged, respectively, by the discrimination index and
482 spontaneous alternation percentage in the spontaneous alternation test in a Y-maze (Y-SAT)
483 (Fig. 3G,H). Next, we examined long-term spatial learning and reference memory using the
484 Morris water maze (MWM). During the training sessions with the hidden platform version of
485 the test, performance improved significantly in both groups, although escape latency in
486 mutant mice remained significantly higher compared to WT littermates (Fig. 3I). During the
487 probe trial on day 8, *Kdm5b^{ΔΔ}* mice displayed a reduced number of platform crossings (Fig.
488 3J), indicating impaired spatial memory. All groups of mice explored the target quadrant
489 significantly more than other quadrants during the probe trial, indicating that spatial memory
490 had been acquired, but homozygous females showed significantly reduced exploration time
491 in the target quadrant compared to wildtype females (Fig. 3K), consistent with a deficit in
492 spatial learning. There was no effect on swim speed during the Morris water maze test,
493 excluding a reduction in the ability of mice to explore the water maze as a potential
494 explanation for the reduced performance of the mutants (Fig. 3L). No significant differences
495 were observed between genotypes in the visible platform task in male mice, excluding poor
496 vision, altered motivation or sensorimotor alterations as a cause for the deficit in mutant
497 male mice. However, an increased latency to find the visible platform was observed in

498 females (Fig. 3M), which might be indicative of visual or motivation changes, or subtle
499 anxiety differences that could be contributing to the deficits observed during the training and
500 testing sessions. Grip strength analysis revealed reduced front- and hindlimb strength in
501 mutant mice (Fig. 3N,O). Finally, we performed the contextual fear conditioning test to
502 assess associative long-term memory. During the training session, both groups of mice
503 increased their freezing behaviour following three unconditioned stimuli (US) of 0.7 mA, 2 s
504 foot shocks) (Fig. 3P). However, freezing behaviour was significantly reduced in *Kdm5b^{ΔΔ}*
505 mice compared to their wildtype littermates. In the testing session 24 h later, reduced
506 freezing was observed on the mutant animals (Fig. 3Q). The increased movement during the
507 training session was also observed when tracking the animals' movement, but their mean
508 speed was similar during the shock administration, excluding differences in the ability of
509 mutants to discern or respond to the shock (Fig. 3R). Nevertheless, the hyperactive
510 phenotype in these mice (see Fig. 3B) should be considered as an inevitable confounding
511 factor on this test. In summary, although the hyperactivity of the mutants complicates the
512 interpretation of the contextual fear conditioning test, and confounds exist for the Morris
513 water maze, *Kdm5b^{ΔΔ}* mice exhibited clear deficits in the hippocampus-dependent object
514 location task, with no confounds apparent, leading us to conclude that these mice exhibit
515 hippocampus-dependent learning and memory deficits

516

517 **Altered baseline and learning-induced hippocampal gene expression in *Kdm5b^{ΔΔ}*** 518 **mice**

519 As KDM5B regulates gene transcription, we next asked if reduced KDM5B demethylase
520 activity affected the transcriptional landscape in the mouse hippocampus. We performed
521 RNA sequencing of adult wild-type and homozygous hippocampi. We detected 20
522 differentially expressed genes (DEGs), of which 14 were up- and 6 were down-regulated
523 (Fig. 4A, B and Extended data Table 4-1). Intriguingly, two key early response genes
524 associated with learning and memory, *Egr1* and *Npas4*, were amongst the downregulated

525 genes (Fig. 4B). To validate this finding, we quantified transcripts for several immediate early
526 genes (*Egr1*, *Npas4*, *cFos*, *Egr2* and *Arc*) by quantitative PCRs (qRT-PCR) from a separate
527 set of hippocampal samples. Consistent with the RNA-seq data, the expression of *Egr1*,
528 *Npas4* and *cFos* were significantly downregulated in the mutants (Fig. 4B). We next asked if
529 these results translated into alterations in protein levels. As *Npas4* is specifically and
530 selectively induced by neuronal activity in the CA3 and DG regions of the hippocampus
531 (Ramamoorthi et al., 2011), *Npas4*-positive cells were quantified by immunostaining. The
532 number of *Npas4*-positive cells was reduced in *Kdm5b*^{Δ/Δ} mice compared to their wildtype
533 littermates (Fig. 4D,E).

534 Activity-dependent transcription factors such as *Npas4* are crucial for memory formation
535 (Weng et al., 2018; Sun et al., 2020). Thus, we decided to test if KDM5B deficiency is
536 associated with abnormal activity-dependent gene regulation during hippocampus-
537 dependent learning. We compared the hippocampal transcriptomes of three groups of mice
538 with RNA-seq: naïve animals, and mice that were sacrificed 1h or 3h following training in the
539 contextual fear conditioning (CFC) paradigm (see Extended data Fig. 5-1 and Table 5-1). As
540 validation, we were again able to confirm the reduction of immediate early gene expression
541 by qRT-PCR in these samples (Extended data Fig. 5-1A). To understand the differences in
542 activity-induced transcriptional responses between wildtype and mutant mice, we clustered
543 the differentially expressed genes by k-means clustering according to their trajectories
544 (Extended data Table 5-2). Four different clusters were identified, referred to as Clusters 1-4
545 below. Cluster 1 exemplified a typical immediate early gene trajectory of rapid, transient
546 induction at 1h (Fig. 5A). These genes were functionally enriched for transcriptional
547 regulation (Extended data Fig. 5-1G), consistent with the fact that the majority of these
548 genes encode transcriptional factors like *c-Fos*, *Fosb*, *Egr1*, *Egr2* and *Npas4*. In agreement
549 with our previous experiments (Fig. 4), this analysis revealed that Cluster 1 genes were
550 downregulated in naïve, control mutant animals, compared to wildtypes (Fig. 5A). These
551 genes were rapidly induced in mutants, to a larger extent than in wildtypes, such that they

552 were expressed at the same level as wildtype controls at both 1h and 3h post-CFC (Fig. 5A).
553 This observation was confirmed by qRT-PCR for the immediate early genes: *Egr2*, *cFos*,
554 *Egr1*, *Npas4* and *Arc* (Extended data Fig. 5-1B-F).

555

556 We detected three other clusters with different trajectories (Fig. 5B-D). Cluster 2 genes
557 showed an induction that gradually increased over time after the learning stimulus (Fig. 5B).
558 These genes included late response genes, some with known functions in neurogenesis and
559 synaptic plasticity e.g. *Fgfr1* (Zhao et al., 2007). Similar to Cluster 1, Cluster 2 genes were
560 downregulated in mutants at baseline, and reached similar expression levels to wildtype
561 controls by 3h (Fig. 5B). Cluster 3 included genes that were constitutively overexpressed in
562 homozygous mutants (Fig. 5C). This cluster was enriched for transcriptional regulation and
563 cation binding proteins and included genes encoding transcription factors such as *Stat4* and
564 *Stat6*, as well as Zn finger proteins. These genes included *Cacna1i*, a gene encoding a
565 calcium channel subunit. Gain-of-function mutations in this gene associated with
566 neurodevelopmental disorders and epilepsy (El Ghaleb et al., 2021). Cluster 3 also included
567 *C1ql2* and *C1ql3*, encoding complement proteins strongly expressed in mossy fibres with a
568 crucial role in the control of synapse stability and number (Matsuda et al., 2016). Cluster 4
569 genes represented genes that were downregulated in response to a learning stimulus in both
570 wildtype and mutant hippocampi, with the downregulation more pronounced in mutants (Fig.
571 5D). This cluster was enriched for transcriptional and signalling regulators (Extended data
572 Fig. 5-1G). Interestingly, these included the *Pde10a* gene, known to enhance fear memories
573 in certain contexts e.g. (Guo et al., 2016), but also genes like *Hgf* known to promote learning
574 and memory, perhaps providing an explanation of learning deficits in our KDM5B mutant
575 mice (Kato et al., 2012). Cluster 4 also includes *Top1*, whose inhibition leads to reduced
576 transcription of genes associated with ASD and neurotransmission regulation (Mabb et al.,
577 2014), and *Arid1b*, which is also implicated in ASD and ID (Moffat et al., 2022).

578

579 To better understand how gene expression varied between genotypes at the different time
580 points, we visualised genes differentially expressed between WT and mutant samples at
581 baseline (home cage test-naive, 0h), 1h and 3h after fear conditioning stimulus. Naive mice
582 showed a small number of DEGs between genotypes (Fig. 5E, 12 DEGs). More DEGs were
583 observed between genotypes in activity-induced transcriptional responses 1h (Fig. 5F, 106
584 DEGs) and 3h (Fig. 5G, 32 DEGs) after training. The majority of DEGs in all conditions were
585 upregulated in the mutant animals, in both female and male mice (Fig. 5E-G), consistent with
586 KDM5B acting as a transcriptional repressor.

587 To understand how the activity-induced transcriptional responses differed between wildtype
588 and mutants, we compared the hippocampal transcriptomes of homecage control mice with
589 mice 1h and 3h post-US. Wildtype animals showed the expected increase in expression of
590 activity-dependent immediate early genes such as *Fosb*, *Npas4* and *Egr3* 1h after training
591 (Fig. 5H, 1h). Three hours after training, gene expression levels of activity genes were back
592 to baseline (Fig. 5H, 3h), consistent with previous studies (Deliu et al., 2018). In addition to
593 the immediate early genes observed in wildtype mice, *Kdm5b*^{Δ/Δ} mice displayed a marked
594 upregulation of many more genes (Fig. 5I, 1h; 252 DEGs). Strikingly, three hours after
595 training, >200 genes were still differentially expressed, including immediate early genes like
596 *Fosb*, *Nr4a2* and *Egr3* (Fig. 5I, 3h; 240 DEGs and Extended data Fig. 5-1H-J). Together,
597 these data shows that reduced KDM5B demethylase activity alters the transcriptional
598 landscape in the hippocampus in a number of different ways. These include downregulated
599 baseline levels of immediate early genes, and more pronounced and sustained activity-
600 dependent upregulation following learning relative to these baseline levels. In conclusion,
601 the abnormal expression of several classes of genes implicated in learning and memory in
602 the hippocampus are likely to contribute to the hippocampus-dependent learning deficits in
603 these mice.

604

605

606 **KDM5B directly regulates learning and memory in the adult hippocampus**

607 Our data thus far suggested that KDM5B has a direct role in learning and memory. However,
608 as KDM5B is known to play important roles during development (Catchpole et al., 2011;
609 Albert et al., 2013), the phenotypes observed in *Kdm5b*^{ΔΔ} mice and other *Kdm5b*-deficient
610 mouse models (Martin et al., 2018; Chen et al., 2023), might all be secondary to abnormal
611 brain development and maturation. To determine if KDM5B has a direct role in learning and
612 memory in the adult brain, we knocked down *Kdm5b* expression in the dorsal hippocampus
613 (CA1) of adult mice by AAV-mediated delivery of a *Kdm5b*-specific shRNA (Fig. 6A,B).

614 A quantification of *Kdm5b* mRNA over time by qRT-PCR, showed a significant knockdown of
615 *Kdm5b* by 3 weeks after viral delivery, and beginning to return to normal levels by 7 weeks
616 (Fig. 6C). Importantly, we observed a shKDM5B-dependent downregulation of immediate
617 early genes in naïve animals compared to controls that received AAV with a scrambled
618 shRNA (Fig. 6D). This observation suggests that the reduced expression of these immediate
619 early genes in *Kdm5b*^{ΔΔ} mice (see Fig. 4) are not secondary to developmental abnormalities.
620 *Kdm5b* knockdown (shRNA) mice showed a significant hyperactivity phenotype in the open
621 field versus controls (Fig. 6E), recapitulating observations with *Kdm5b*^{ΔΔ} mice (see Fig. 3B).
622 Importantly, *Kdm5b* knockdown resulted in a substantial deficit in hippocampus-dependent
623 learning and memory in the OLM task (Fig. 6F), similar to those in *Kdm5b*^{ΔΔ} mice, indicating
624 that *Kdm5b* is essential for normal long-term memory consolidation in the hippocampus.
625 Exploration time did not show differences between groups in neither training nor testing
626 sessions (Student's t-test: p=0.4940 for training, and p=0.1242 for testing). Furthermore, the
627 shRNA mice exhibited a striking incidence of spontaneous seizures (Fig. 6G), suggesting
628 that *Kdm5b* knockdown altered neuronal activation and/or circuitry in the hippocampus.

629

630 **Kdm5b regulates synaptic plasticity**

631 To determine if *Kdm5b* knock-down affected synaptic plasticity, we examined short- and
632 long-term potentiation (LTP) in acute hippocampal slices from these mice. We measured
633 LTP in the dorsal CA1b region of the hippocampus, which we have found to be critically
634 important for the hippocampus-dependent object location memory task in previous studies
635 (Barrett et al., 2011; Vogel-Ciernia et al., 2013). Theta burst stimulation produced an
636 immediate increase in potentiation in slices from control mice that gradually decayed to a
637 plateau level that was approximately 50% above pre-TBS baseline (Fig. 6H). Hippocampal
638 slices prepared from *Kdm5b* shRNA mice had similar short-term potentiation to control
639 slices, however, the LTP was significantly less stable as the potentiation fell below control
640 levels 1h post-theta burst stimulation. The mean potentiation for the last 10 min of 1h post-
641 theta burst stimulation was $31 \pm 11\%$ for *Kdm5b* shRNA slices and $47 \pm 6\%$ for control slices
642 (Fig. 6I), suggesting that *Kdm5b* is necessary for the consolidation of LTP in area CA1 of the
643 hippocampus.

644

645 We tested whether synaptic events leading to induction of LTP are negatively affected by
646 *Kdm5b* knock-down by measuring short-term plasticity changes including input/output curves
647 (i/o) and paired-pulse facilitation. The input/output curves were comparable for controls and
648 *Kdm5b* shRNA mice (Fig. 6J). The slope of the io curves was not significantly different
649 between groups ($p < 0.90$, data not shown). Paired-pulse facilitation (Fig. 6K), a measure of
650 transmitter release kinetics, also did not show any significant difference between groups and
651 stimulus intervals (2 way-ANOVA; $F_{(2,28)} = 2.28$, $p < 0.12$). Thus, it appears that the lack of
652 stability in LTP upon *Kdm5b* knockdown involves cellular events that are set in motion after
653 induction and expression of LTP, an interpretation that is consistent with the observation that
654 short-term potentiation was unaffected in both groups of mice.

655

656

658 **Discussion**

659 Rare coding variants in *KDM5B* are associated with cognitive function in adults and *KDM5B*
660 is associated with a recessive intellectual disability disorder (Faundes et al., 2018; Martin et
661 al., 2018; Chen et al., 2023). In this manuscript, we show that mice homozygous for a
662 hypomorphic allele of *Kdm5b* that lacks H3K4me3 demethylase activity exhibited learning
663 and memory deficits. *Kdm5b* deficiency resulted in alterations in the expression of genes
664 implicated in learning and memory. Acute knockdown experiments showed that *Kdm5b* is
665 critical for normal function of the hippocampus after development has been completed.
666 Notably, two individuals carrying *KDM5B* variants show epileptic spasms and/or generalized
667 seizures (Martin et al., 2018; Mangano et al., 2022), although the latter is more likely
668 associated with a deficit in *Nav1*. Following *Kdm5b* knockdown in the dorsal hippocampus of
669 adult mice, mice exhibited seizures, consistent with an essential role for *Kdm5b* in
670 maintaining normal circuit homeostasis. These mice had deficits in hippocampus-dependent
671 learning and memory and LTP. Together, this study provides a significant advance in our
672 understanding of the role of KDM5B in learning and memory. Our findings show that KDM5B
673 functions in the adult hippocampus to control learning and memory and imply that at least
674 some of the cognitive deficits associated with KDM5B deficiency could be amenable to
675 treatment in adults.

676

677 **Learning and memory genes regulated by KDM5B**

678 Our gene expression analyses revealed several potential ways in which KDM5B deficiency
679 might disrupt memory and learning. First, the expression of activity-dependent, immediate
680 early genes was reduced in *Kdm5b^{Δ/Δ}* mice. The deletion of several of these genes have
681 been shown to affect long-term memory formation, whilst leaving short-term memory intact
682 (Jones et al., 2001; Fleischmann et al., 2003; Ramamoorthi et al., 2011), similar to our
683 findings with *Kdm5b^{Δ/Δ}* mice. Second, we found that these immediate early genes were

684 induced by neuronal activation in the hippocampus of *Kdm5b* mutants up to levels equivalent
685 to those in wildtype mice, and therefore hyper-activated relative to baseline levels.
686 Furthermore, these genes were still expressed 3h after neuronal activation in the mutants, at
687 a time point when their expression has returned to baseline in wildtype mice. This inability of
688 gene expression to return to baseline levels is consistent with the H3K4me3 demethylase
689 function of KDM5B. One might speculate that this reduced expression at baseline and
690 apparent over-activation and altered dynamics of IEGs might disrupt normal memory
691 allocation and consolidation mechanisms in *Kdm5b* mutants, theories that need to be tested
692 for *Kdm5b* and other related disorders (Han et al., 2007; Han et al., 2008). For instance,
693 Deliu et al. reported altered trajectories of gene expression in response to conditioning in
694 *Setd5* mutant mice, albeit that baseline gene expression was not markedly different in these
695 mutants compared to wildtype controls (Deliu et al., 2018). Third, *Kdm5b* mutant animals
696 also showed an abnormal overexpression of a cluster of genes that was not affected by
697 neural activity. This cluster, which included proteins with a regulatory role over synaptic
698 function and transcription regulation factors include those genes constitutively affected by
699 the lack of KDM5B demethylase activity. Our results also implicate KDM5B in the regulation
700 of gene transcription through a number of zinc finger proteins, e.g. Zfx2, Zfx1, Zbtb22 and
701 Zfp810, whose expression is either constitutively affected or abnormally downregulated upon
702 learning in mutant mice (Komine et al., 2012).

703

704 Our GOterms analyses also revealed that WT1 is one of the top transcription factors
705 modulating the expression of genes that are downregulated upon a learning stimulus
706 (Cluster 4, see Fig. 5D). A recent study showed that WT1 regulates neuronal excitability,
707 LTP and long-term memory formation. WT1 limits memory strength, thus enabling the
708 memory flexibility required for normal memory formation (Mariottini et al., 2019). The
709 possible relationship between KDM5B and WT1 warrants further investigation.

710

711 Together, these data showed that the expression of several different types and classes of
712 genes that are regulated by neuronal activation and necessary for learning and memory are
713 affected by *Kdm5b* deficiency.

714

715 **H3K4me3 dysregulation in learning and memory**

716 The finding that mice with *Kdm5b* knockdown in the adult hippocampus exhibit long-term
717 memory deficits, suggests that KDM5B has a direct role in learning and memory,
718 independent from any developmental functions. The most likely mechanism is that a
719 deficiency in KDM5B demethylase activity impacts H3K4me3 dynamics and transcriptional
720 output of key learning-associated genes (Gupta et al., 2010; Collins et al., 2019b; Collins et
721 al., 2019a). Abnormalities may be present in different brain regions and cell types and during
722 distinct stages of memory formation, such as allocation (Han et al., 2007; Han et al., 2008),
723 consolidation (Gupta et al., 2010) and retrieval (Webb et al., 2017). Thus, future studies may
724 need to assess H3K4me3 dynamics at specific gene promoters in different cell types. The
725 conditional deletion of *Kmt2a* and *Kmt2b* in post-mitotic neurons using CamKIIcre was
726 sufficient to cause hippocampus-dependent learning and memory deficits, suggesting a
727 direct role for these genes in excitatory neurons (Kerimoglu et al., 2017). Together, these
728 findings further support the notion that H3K4me3 regulation is important for learning and
729 memory and suggest that dysregulation of H3K4me3, in either direction, can lead to memory
730 deficits. However, as chromatin regulators typically function in large, multi-molecular
731 complexes, other mechanistic explanations cannot be ruled out. Furthermore, a direct
732 comparison between genes regulated by *Kmt2a* and *Kmt2b* has shown that these factors
733 regulate different genes that likely impact neuronal plasticity in distinct ways (Kerimoglu et
734 al., 2017). The two other H3K4me3-specific demethylases, KDM5A and KDM5C have also
735 been implicated in learning and memory. A *Kdm5a*^{-/-} mouse model was shown to exhibit
736 deficits in the Morris water maze and *Kdm5c*^{-/-} mice have deficits in contextual fear memory
737 and novel object recognition (El Hayek et al., 2020; Vallianatos et al., 2020). Aguilar-Valles
738 et al. have shown that *Kdm5c* knock-down in the nucleus accumbens in adult mice results in

739 increased H3K4me3 at gene promoters and deficits in methamphetamine-associated
740 memory formation (Aguilar-Valles et al., 2014). To the best of our knowledge, *Kdm5a* has
741 not yet been deleted or knocked down in post-mitotic neurons in the adult brain, so direct
742 functions for this factor in learning and memory still need to be formally proven. Intriguingly,
743 the contextual fear memory deficits in *Kmt2a*^{+/-} and *Kdm5c*^{-/-} mice were rescued in *Kmt2a*^{+/-}
744 ;*Kdm5c*^{-/-} double heterozygous mice, suggesting that these factors regulated the same or
745 similar processes, but in opposite directions (Vallianatos et al., 2020).

746

747 **Cellular/synaptic functions of KDM5B**

748 Mouse models for other H3K4me regulators such as *Kmt2a*, *Kdm5c*, *Kdm5a* or *Set1a*
749 display both memory deficits and a decrease in spine density in the hippocampus or cortex
750 (Mukai et al., 2019; El Hayek et al., 2020; Vallianatos et al., 2020). We did not detect
751 significant changes in spine number in the hippocampal stratum oriens and radiatum, or
752 stratum moleculare in the *Kdm5b* mutant mice, suggesting that overt changes in excitatory
753 spine density might not account for the memory deficits in these mutants. The LTP deficit
754 appears to be due to postsynaptic abnormalities, because we did not find any alternations in
755 presynaptic transmitter release. Future studies will need to examine postsynaptic membrane
756 proteins that are known to be involved in LTP and their potential regulation by KDM5B-
757 dependent mechanisms. The exact cell types affected by *Kdm5b* deficiency will also need to
758 be determined.

759

760 We recognise certain limitations in our study. We set out to test if KDM5B demethylase
761 activity have a role in long-term memory consolidation. Although our results are consistent
762 with this hypothesis, KDM5B protein levels were also downregulated in *Kdm5b*^{ΔΔ} mice,
763 limiting our ability to conclusively ascertain the contribution of demethylase deficiency vs.
764 other KDM5B functions. However, it is also intriguing to note that mutations affecting the

765 demethylase activity of *Drosophila* KDM5 leads to memory deficits and decreases
766 neurotransmission (Zamurrad et al., 2018; Belalcazar et al., 2021).

767

768 The relevance of the increased seizures in *Kdm5b* knock-down mice to clinical phenotypes
769 associated with KDM5B deficiency is still unclear. Chen *et al.* recently reported protein
770 truncating variants of *KDM5B* in individuals with epilepsy, but so far, the clinical description
771 of the small number of individuals with recessive *KDM5B* intellectual disability syndrome has
772 not revealed a significant association (Faundes et al., 2018; Martin et al., 2018). We have
773 not observed an obvious increase in spontaneous seizures in our homozygous mouse
774 model. One possibility is that KDM5B deficiency throughout development allows for sufficient
775 homeostatic compensatory mechanisms to ameliorate an overt excitatory/inhibitory
776 imbalance that might lead to spontaneous seizures in some individuals.

777

778 Mutations in chromatin modifying and remodelling factors represent a significant proportion
779 of mutations associated with neurodevelopmental disorders and intellectual disability
780 (Valencia et al., 2023). The functions of most of these factors in the developing and adult
781 brain are still unknown. As these factors are pleiotropic and likely regulates multiple
782 developmental processes and functions in the brain, identifying their salient functions and
783 mechanisms of action remain a significant challenge. This study, together with other recent
784 reports on other chromatin remodelling factors (Kerimoglu et al., 2013; Vogel-Ciernia et al.,
785 2013; Kerimoglu et al., 2017; Chen et al., 2023), suggest that these factors play central roles
786 in the regulation of genes necessary for learning and memory and that intellectual disability
787 disorders and cognitive deficits caused by mutation of these factors may to some extent be
788 caused by direct roles in postmitotic neurons. Reduced function of these factors appears to
789 be associated with altered trajectories of activity-dependent gene expression and abnormal
790 engagement of downstream synaptic plasticity mechanisms (Deliu et al., 2018).

791 Understanding these pathological mechanisms may lead to the development of targeted and
792 improved therapies for intellectual disability disorders.

793

794

795

796

797

JNeurosci Accepted Manuscript

798 **Study approval**

799 All animal work were approved by local ethical review panels (AWERB, King's College
800 London) and IACUC (UCI 20-095) and work conducted in the UK approved by a Home
801 Office Project licence (PP6246123).

802

803 **Data availability**

804 RNAseq data (fastq files) were deposited at the Gene Expression Omnibus (GEO) archive
805 under the accession number GSE240887 and made freely available upon publication.

806

807 **Author contributions**

808 MAB, KPG, MAW and LPS conceived the study and designed the experiments and LCA,
809 CF, MAW, KPG and MAB supervised the research. LPS, SB, RM, TG and MAB performed
810 behavioural studies, EK performed LTP experiments, LPS, AG, JAC and AMP performed
811 bioinformatic analyses, FGG, AK and MAB performed surgeries for shRNA knockdown and
812 DPM performed qRT-PCR experiments. LPS, EK and MAB wrote the manuscript with input
813 from co-authors.

814

815 **Acknowledgements**

816 We thank Joyce Taylor-Papadimitriou for sharing the *Kdm5b* mouse line, animal husbandry
817 staff at KCL and UCI for expert animal care, and Agatha Sahra Augustynski for technical
818 assistance. This work was supported by grants from the MRC (MR/V013173/1 to MAB and
819 KPG and MR/X010481/1 to LCA and MAB) and National Institute of Aging grants AG057558
820 to MAW, AG076835 to MAW, K99AG078501 to AAK, AG077872 to FGG. SB is supported
821 by an MRC DTP iCASE PhD studentship and AG by the Wellcome Trust NIIHD PhD
822 programme. MAB received funding for a sabbatical in the Wood laboratory from the Faculty
823 of Dental, Craniofacial and Oral Sciences at KCL.

824

825 The Galaxy server that was used for some of the bioinformatic analyses is in part funded by
826 Collaborative Research Centre 992 Medical Epigenetics (DFG grant SFB 992/1 2012) and
827 German Federal Ministry of Education and Research (BMBF grants 031 A538A/A538C RBC,
828 031L0101B/031L0101C de.NBI-epi, 031L0106 de.STAIR (de.NBI).

829

830

831

JNeurosci Accepted Manuscript

833 References

834

835

836 Aguilar-Valles A, Vaissiere T, Griggs EM, Mikaelsson MA, Takacs IF, Young EJ, Rumbaugh G, Miller CA
837 (2014) Methamphetamine-associated memory is regulated by a writer and an eraser of
838 permissive histone methylation. *Biol Psychiatry* 76:57-65.

839 Albert M, Schmitz SU, Kooistra SM, Malatesta M, Morales Torres C, Rekling JC, Johansen JV,
840 Abarrategui I, Helin K (2013) The histone demethylase Jarid1b ensures faithful mouse
841 development by protecting developmental genes from aberrant H3K4me3. *PLoS Genet*
842 9:e1003461.

843 Bankhead P, Loughrey MB, Fernandez JA, Dombrowski Y, McArt DG, Dunne PD, McQuaid S, Gray RT,
844 Murray LJ, Coleman HG, James JA, Salto-Tellez M, Hamilton PW (2017) QuPath: Open source
845 software for digital pathology image analysis. *Sci Rep* 7:16878.

846 Barrett RM, Malvaez M, Kramar E, Matheos DP, Arrizon A, Cabrera SM, Lynch G, Greene RW, Wood
847 MA (2011) Hippocampal focal knockout of CBP affects specific histone modifications, long-
848 term potentiation, and long-term memory. *Neuropsychopharmacology* 36:1545-1556.

849 Belalcazar HM, Hendricks EL, Zamurra S, Liebl FLW, Secombe J (2021) The histone demethylase
850 KDM5 is required for synaptic structure and function at the *Drosophila* neuromuscular
851 junction. *Cell Rep* 34:108753.

852 Catchpole S, Spencer-Dene B, Hall D, Santangelo S, Rosewell I, Guenatri M, Beatson R, Scibetta AG,
853 Burchell JM, Taylor-Papadimitriou J (2011) PLU-1/JARID1B/KDM5B is required for embryonic
854 survival and contributes to cell proliferation in the mammary gland and in ER+ breast cancer
855 cells. *Int J Oncol* 38:1267-1277.

856 Chen CY et al. (2023) The impact of rare protein coding genetic variation on adult cognitive function.
857 *Nat Genet.*

858 Chen PB, Kawaguchi R, Blum C, Achiro JM, Coppola G, O'Dell TJ, Martin KC (2017) Mapping Gene
859 Expression in Excitatory Neurons during Hippocampal Late-Phase Long-Term Potentiation.
860 *Front Mol Neurosci* 10:39.

861 Collins BE, Sweatt JD, Greer CB (2019a) Broad domains of histone 3 lysine 4 trimethylation are
862 associated with transcriptional activation in CA1 neurons of the hippocampus during
863 memory formation. *Neurobiology of learning and memory* 161:149-157.

864 Collins BE, Greer CB, Coleman BC, Sweatt JD (2019b) Histone H3 lysine K4 methylation and its role in
865 learning and memory. *Epigenetics Chromatin* 12:7.

866 Deliu E, Arecco N, Morandell J, Dotter CP, Contreras X, Girardot C, Kasper EL, Kozlova A, Kishi K,
867 Chiaradia I, Noh KM, Novarino G (2018) Haploinsufficiency of the intellectual disability gene
868 SETD5 disturbs developmental gene expression and cognition. *Nat Neurosci* 21:1717-1727.

869 El Ghaleb Y, Schneeberger PE, Fernandez-Quintero ML, Geisler SM, Pelizzari S, Polstra AM, van
870 Hagen JM, Denecke J, Campiglio M, Liedl KR, Stevens CA, Person RE, Rentas S, Marsh ED,
871 Conlin LK, Tuluc P, Kutsche K, Flucher BE (2021) CACNA1I gain-of-function mutations
872 differentially affect channel gating and cause neurodevelopmental disorders. *Brain : a*
873 *journal of neurology* 144:2092-2106.

874 El Hayek L et al. (2020) KDM5A mutations identified in autism spectrum disorder using forward
875 genetics. *eLife* 9.

876 Faundes V et al. (2018) Histone Lysine Methylases and Demethylases in the Landscape of Human
877 Developmental Disorders. *Am J Hum Genet* 102:175-187.

878 Fleischmann A, Hvalby O, Jensen V, Strelakova T, Zacher C, Layer LE, Kvello A, Reschke M, Spanagel
879 R, Sprengel R, Wagner EF, Gass P (2003) Impaired long-term memory and NR2A-type NMDA
880 receptor-dependent synaptic plasticity in mice lacking c-Fos in the CNS. *J Neurosci* 23:9116-
881 9122.

882 Gildea JJ, Lopez R, Shearn A (2000) A screen for new trithorax group genes identified little imaginal
883 discs, the *Drosophila melanogaster* homologue of human retinoblastoma binding protein 2.
884 *Genetics* 156:645-663.

885 Guo L, Guo Z, Luo X, Liang R, Yang S, Ren H, Wang G, Zhen X (2016) Phosphodiesterase 10A inhibition
886 attenuates sleep deprivation-induced deficits in long-term fear memory. *Neurosci Lett*
887 635:44-50.

888 Gupta S, Kim SY, Artis S, Molfese DL, Schumacher A, Sweatt JD, Paylor RE, Lubin FD (2010) Histone
889 methylation regulates memory formation. *J Neurosci* 30:3589-3599.

890 Han JH, Yiu AP, Cole CJ, Hsiang HL, Neve RL, Josselyn SA (2008) Increasing CREB in the auditory
891 thalamus enhances memory and generalization of auditory conditioned fear. *Learn Mem*
892 15:443-453.

893 Han JH, Kushner SA, Yiu AP, Cole CJ, Matynia A, Brown RA, Neve RL, Guzowski JF, Silva AJ, Josselyn SA
894 (2007) Neuronal competition and selection during memory formation. *Science* 316:457-460.

895 Hughes AL, Kelley JR, Klose RJ (2020) Understanding the interplay between CpG island-associated
896 gene promoters and H3K4 methylation. *Biochim Biophys Acta Gene Regul Mech*
897 1863:194567.

898 Hurley S, Mohan C, Suetterlin P, Ellingford R, Riegman KLH, Ellegood J, Caruso A, Michetti C, Brock O,
899 Evans R, Rudari F, Delogu A, Scattoni ML, Lerch JP, Fernandes C, Basson MA (2021) Distinct,
900 dosage-sensitive requirements for the autism-associated factor CHD8 during cortical
901 development. *Mol Autism* 12:16.

902 Jamshidi S, Catchpole S, Chen J, So CWE, Burchell J, Rahman KM, Taylor-Papadimitriou J (2021)
903 KDM5B protein expressed in viable and fertile DeltaARID mice exhibit no demethylase
904 activity. *Int J Oncol* 59.

905 Jones MW, Errington ML, French PJ, Fine A, Bliss TV, Garel S, Charnay P, Bozon B, Laroche S, Davis S
906 (2001) A requirement for the immediate early gene *Zif268* in the expression of late LTP and
907 long-term memories. *Nat Neurosci* 4:289-296.

908 Jones WD, Dafou D, McEntagart M, Woollard WJ, Elmslie FV, Holder-Espinasse M, Irving M, Sagar
909 AK, Smithson S, Trembath RC, Deshpande C, Simpson MA (2012) De novo mutations in MLL
910 cause Wiedemann-Steiner syndrome. *Am J Hum Genet* 91:358-364.

911 Kato T, Funakoshi H, Kadoyama K, Noma S, Kanai M, Ohya-Shimada W, Mizuno S, Doe N, Taniguchi T,
912 Nakamura T (2012) Hepatocyte growth factor overexpression in the nervous system
913 enhances learning and memory performance in mice. *J Neurosci Res* 90:1743-1755.

914 Kerimoglu C, Agis-Balboa RC, Kranz A, Stilling R, Bahari-Javan S, Benito-Garagorri E, Halder R,
915 Burkhardt S, Stewart AF, Fischer A (2013) Histone-methyltransferase MLL2 (KMT2B) is
916 required for memory formation in mice. *J Neurosci* 33:3452-3464.

917 Kerimoglu C, Sakib MS, Jain G, Benito E, Burkhardt S, Capece V, Kaurani L, Halder R, Agis-Balboa RC,
918 Stilling R, Urbanke H, Kranz A, Stewart AF, Fischer A (2017) KMT2A and KMT2B Mediate
919 Memory Function by Affecting Distinct Genomic Regions. *Cell Rep* 20:538-548.

920 Komine Y, Takao K, Miyakawa T, Yamamori T (2012) Behavioral abnormalities observed in *Zfhx2*-
921 deficient mice. *PLoS One* 7:e53114.

922 Kwapis JL, Alagband Y, Kramar EA, Lopez AJ, Vogel Ciernia A, White AO, Shu G, Rhee D, Michael CM,
923 Montellier E, Liu Y, Magnan CN, Chen S, Sassone-Corsi P, Baldi P, Matheos DP, Wood MA
924 (2018) Epigenetic regulation of the circadian gene *Per1* contributes to age-related changes in
925 hippocampal memory. *Nature communications* 9:3323.

926 Lauberth SM, Nakayama T, Wu X, Ferris AL, Tang Z, Hughes SH, Roeder RG (2013) H3K4me3
927 interactions with TAF3 regulate preinitiation complex assembly and selective gene
928 activation. *Cell* 152:1021-1036.

929 Liu X, Secombe J (2015) The Histone Demethylase KDM5 Activates Gene Expression by Recognizing
930 Chromatin Context through Its PHD Reader Motif. *Cell Rep* 13:2219-2231.

931 Mabb AM, Kullmann PH, Twomey MA, Miriyala J, Philpot BD, Zylka MJ (2014) Topoisomerase 1
932 inhibition reversibly impairs synaptic function. *Proc Natl Acad Sci U S A* 111:17290-17295.

933 Mangano GD, Antona V, Cali E, Fontana A, Salpietro V, Houlden H, Veggiotti P, Nardello R (2022) A
934 complex epileptic and dysmorphic phenotype associated with a novel frameshift KDM5B
935 variant and deletion of SCN gene cluster. *Seizure* 97:20-22.

936 Mariottini C, Munari L, Gunzel E, Seco JM, Tzavaras N, Hansen J, Stern SA, Gao V, Aleyasin H, Sharma
937 A, Azeloglu EU, Hodes GE, Russo SJ, Huff V, Birtwistle MR, Blitzer RD, Alberini CM, Iyengar R
938 (2019) Wilm's tumor 1 promotes memory flexibility. *Nature communications* 10:3756.

939 Martin HC et al. (2018) Quantifying the contribution of recessive coding variation to developmental
940 disorders. *Science* 362:1161-1164.

941 Matsuda K, Budisantoso T, Mitakidis N, Sugaya Y, Miura E, Kakegawa W, Yamasaki M, Konno K,
942 Uchigashima M, Abe M, Watanabe I, Kano M, Watanabe M, Sakimura K, Aricescu AR, Yuzaki
943 M (2016) Transsynaptic Modulation of Kainate Receptor Functions by C1q-like Proteins.
944 *Neuron* 90:752-767.

945 Moffat JJ, Smith AL, Jung EM, Ka M, Kim WY (2022) Neurobiology of ARID1B haploinsufficiency
946 related to neurodevelopmental and psychiatric disorders. *Mol Psychiatry* 27:476-489.

947 Mukai J, Cannavo E, Crabtree GW, Sun Z, Diamantopoulou A, Thakur P, Chang CY, Cai Y, Lomvardas S,
948 Takata A, Xu B, Gogos JA (2019) Recapitulation and Reversal of Schizophrenia-Related
949 Phenotypes in *Setd1a*-Deficient Mice. *Neuron* 104:471-487 e412.

950 Ramamoorthi K, Fropf R, Belfort GM, Fitzmaurice HL, McKinney RM, Neve RL, Otto T, Lin Y (2011)
951 *Npas4* regulates a transcriptional program in CA3 required for contextual memory
952 formation. *Science* 334:1669-1675.

953 Sun X, Bernstein MJ, Meng M, Rao S, Sorensen AT, Yao L, Zhang X, Anikeeva PO, Lin Y (2020)
954 Functionally Distinct Neuronal Ensembles within the Memory Engram. *Cell* 181:410-423
955 e417.

956 Valencia AM, Sankar A, van der Sluijs PJ, Satterstrom FK, Fu J, Talkowski ME, Vergano SAS, Santen
957 GWE, Kadoch C (2023) Landscape of mSWI/SNF chromatin remodeling complex
958 perturbations in neurodevelopmental disorders. *Nat Genet.*

959 Vallianatos CN, Raines B, Porter RS, Bonefas KM, Wu MC, Garay PM, Collette KM, Seo YA, Dou Y,
960 Keegan CE, Tronson NC, Iwase S (2020) Mutually suppressive roles of KMT2A and KDM5C in
961 behaviour, neuronal structure, and histone H3K4 methylation. *Commun Biol* 3:278.

962 Vermeulen M, Timmers HT (2010) Grasping trimethylation of histone H3 at lysine 4. *Epigenomics*
963 2:395-406.

964 Vogel-Ciernia A et al. (2013) The neuron-specific chromatin regulatory subunit BAF53b is necessary
965 for synaptic plasticity and memory. *Nat Neurosci* 16:552-561.

966 Wang H, Fan Z, Shliaha PV, Miele M, Hendrickson RC, Jiang X, Helin K (2023) H3K4me3 regulates RNA
967 polymerase II promoter-proximal pause-release. *Nature* 615:339-348.

968 Wang T, Kim CN, Bakken TE, Gillentine MA, Henning B, Mao Y, Gilissen C, Consortium S, Nowakowski
969 TJ, Eichler EE (2022) Integrated gene analyses of de novo variants from 46,612 trios with
970 autism and developmental disorders. *Proc Natl Acad Sci U S A* 119:e2203491119.

971 Webb WM, Sanchez RG, Perez G, Butler AA, Hauser RM, Rich MC, O'Bierne AL, Jarome TJ, Lubin FD
972 (2017) Dynamic association of epigenetic H3K4me3 and DNA 5hmC marks in the dorsal
973 hippocampus and anterior cingulate cortex following reactivation of a fear memory.
974 *Neurobiology of learning and memory* 142:66-78.

975 Weng FJ, Garcia RI, Lutz S, Alvina K, Zhang Y, Dushko M, Ku T, Zemoura K, Rich D, Garcia-Dominguez
976 D, Hung M, Yelhekar TD, Sorensen AT, Xu W, Chung K, Castillo PE, Lin Y (2018) *Npas4* Is a
977 Critical Regulator of Learning-Induced Plasticity at Mossy Fiber-CA3 Synapses during
978 Contextual Memory Formation. *Neuron* 97:1137-1152 e1135.

979 Whittaker DE, Kasah S, Donovan APA, Ellegood J, Riegman KLH, Volk HA, McGonnell I, Lerch JP,
980 Basson MA (2017) Distinct cerebellar foliation anomalies in a CHD7 haploinsufficient mouse
981 model of CHARGE syndrome. *Am J Med Genet C Semin Med Genet* 175.

982 Yheskel M, Sidoli S, Secombe J (2023) Proximity labeling reveals a new in vivo network of interactors
983 for the histone demethylase KDM5. *Epigenetics Chromatin* 16:8.

984 Zamurrad S, Hatch HAM, Drelon C, Belalcazar HM, Secombe J (2018) A Drosophila Model of
985 Intellectual Disability Caused by Mutations in the Histone Demethylase KDM5. Cell Rep
986 22:2359-2369.

987 Zhao M, Li D, Shimazu K, Zhou YX, Lu B, Deng CX (2007) Fibroblast growth factor receptor-1 is
988 required for long-term potentiation, memory consolidation, and neurogenesis. Biol
989 Psychiatry 62:381-390.

990 Zhou X et al. (2022) Integrating de novo and inherited variants in 42,607 autism cases identifies
991 mutations in new moderate-risk genes. Nat Genet 54:1305-1319.

992 Zou MR, Cao J, Liu Z, Huh SJ, Polyak K, Yan Q (2014) Histone demethylase jumonji AT-rich interactive
993 domain 1B (JARID1B) controls mammary gland development by regulating key
994 developmental and lineage specification genes. J Biol Chem 289:17620-17633.

995

996

997

JNeurosci Accepted Manuscript

998 **Figures**

999 **Figure 1. *Kdm5b*^{Δ/Δ} mice express reduced total KDM5B levels and show increased**
1000 **number of H3K4me3-positive cells in the hippocampus**

1001 **A)** Schematics of wildtype (WT) and KDM5B^{ΔARID} protein domains. The mutant allele results
1002 in a truncated carboxyl end of the JmjN domain (JmjN-T) together with a deletion of the
1003 entire ARID domain. **B)** Representative western blot images from WT (+/) and homozygous
1004 (Δ/Δ) mutant mice postnatal day 5 (PND5) hippocampal samples showing the lack of full-
1005 length KDM5B protein in cortical samples from Δ/Δ mice. αTubulin was used as loading
1006 control. Full-length KDM5B (arrowhead) and truncated ΔARID (asterisk) protein bands are
1007 indicated. See Extended data Fig. 1-1 for uncropped blot. Molecular weight (M.W.) markers
1008 in kDa are shown on the left. Female (squares) and male (diamonds) samples are included,
1009 although no sex differences were observed. **C, D)** Quantification of full-length and total (full-
1010 length and truncated) KDM5B protein from B. **E, F)** Quantification of the density of
1011 H3K4me3+ (cyan) cells in the hippocampus of 8 week-old wild-type and mutant mice. Nuclei
1012 were counterstained with DAPI (grey). Scale bar, 50μm. Female (squares) and male
1013 (diamonds) samples are included, although no sex effect was observed. **G, I, K)** Cumulative
1014 frequencies of H3K4me3-positive cells as a function of their staining intensity. Cumulative
1015 probability was calculated including all the detected cells (CA1: 406-903 cells, CA3: 236-925
1016 cells, DG: 925-2491 cells; 4 animals/genotype). **H, J, L)** Representative H3K4me3 (cyan)
1017 immunostaining of hippocampal sections in 8 weeks-old control and mutant mice. Sections
1018 were counterstained with DAPI (grey). Scale bar, 200μm. Data in C, D and F is shown as
1019 mean ±SEM and was analysed with Student's t-test. *p<0.05, **p<0.01.

1020 **Figure 2. *Kdm5b*^{Δ/Δ} homozygous mice are viable but exhibit growth retardation and**
1021 **increased brain:body weight.**

1022 **A)** Homozygous mutants are viable and present at expected Mendelian ratios at P21;
1023 n=128, Chi², p=0.9207. Similar Mendelian rates are observed when analysing males and

1024 females separately (Males: 25.38% +/+, 51.52% Δ/Δ , 23.11% Δ/Δ ; Females: 27.96% +/+,
1025 47.67% Δ/Δ , 24.37% Δ/Δ). **B)** Pre-weaning body weight (g) measurements show decreased
1026 body weight in mutant animals. **C-F)** Body and brain weight, and brain:body and liver:body
1027 weight ratios are shown for +/+ (n=11) and Δ/Δ (n=13) P21 mice. **G)** Representative images
1028 of brains from wildtype and homozygous mutant mice indicating similar sizes. **H)** General
1029 cortical brain architecture is not affected in homozygous animals. Representative images of
1030 cortical brain sections, where nuclei were visualized with Hoechst3332 are shown. Scale
1031 bar, 50 μm ; n=13 +/+ and n=14 Δ/Δ animals. **I)** Layer thickness was measured in the
1032 somatosensory cortex. **J)** Golgi-cox-stained proximal basal and apical dendrites of CA1
1033 pyramidal neurons and apical dendrites of dentate gyrus granule cells in the dorsal
1034 hippocampus were analysed. Graphs depict the average spine density per animal (10-20
1035 dendrites/hippocampal region). Images show representative Golgi-Cox-stained dendrites.
1036 Scale bar, 2.5 μm . N=6 mice/genotype. Data is shown as mean \pm SEM, including female and
1037 male mice. Data was analysed with two-way ANOVA (B, I) or Student's t-test or Mann-
1038 Whitney test when appropriate(C-F, J). *p<0.05, **p<0.01.

1039 **Figure 3. *Kdm5b* ^{Δ/Δ} homozygous mice exhibit hyperlocomotion and learning deficits.**

1040 **A)** Body weight differences in 2 month old mice before the start of the behavioural tests.
1041 Two-way ANOVA genotype effect: ****p<0.0001; sex effect: ***p<0.001. **B)** Distance moved
1042 (cm) in the outer zone of the open field arena. Two-way ANOVA genotype effect:
1043 ***p=0.0005. Three-way ANOVA sex effect: p=0.33. **C)** The amount of time (s) in the inner
1044 zone of the open field is shown. Two-way ANOVA genotype effect: **p=0.0087; sex effect:
1045 *p=0.0107. **D)** Time (%) spent in the open arms in the elevated plus maze (EPM), indicative
1046 of reduced anxiety. Two-way ANOVA genotype effect: p=0.8675, sex effect: p=0.4664. **E)**
1047 Discrimination index (DI) during the training and test (24h) phases in the object location
1048 memory (OLM) test to analyse long term spatial memory. Note significant learning in wild-
1049 type mice compared to training, but no significant learning in *Kdm5b* ^{Δ/Δ} mutants, and the
1050 reduced DI on test session between the two genotypes. Two-way ANOVA interaction effect:

1051 ** $p=0.0057$. Two-way ANOVA sex effect: $p=0.6317$ (training) and $p=0.9086$ (testing) **F)**
1052 There are no genotype differences in total exploration time (s) during training nor testing
1053 session in the OLM test. Two-way ANOVA genotype effect: $p=0.2105$ (training), $p=0.5919$
1054 (testing) and sex effect: $p=0.7506$ (training) and $p=0.2431$ (testing). **G)** DI during the testing
1055 session of the spontaneous alternation in a Y maze (Y-SAT), performed 1 h after training to
1056 assess short-term spatial memory. Two-way ANOVA sex effect: $p=0.0768$. **H)** Spontaneous
1057 alternation rate in the Y-SAT shows no differences between genotypes. **I)** Latency (s) to
1058 reach the hidden platform during the training phase of the Morris water maze (MWM). Data
1059 represents the mean of the 4 trials/day. Two-way ANOVA genotype effect: *** $p=0.0001$.
1060 Three-way ANOVA sex effect: $p=0.0019$. **J, K)** Graphs show the number of platform
1061 crossings (J) and time spent (%) in the different quadrants (K) during the probe trial
1062 performed on day 8. Chance, 25%, is depicted with a dashed line. Two-way ANOVA sex
1063 effect in J: $p=0.3413$. **L)** Swimming speed (cm/s) was similar between genotypes during the
1064 training phase of the MWM. Three-way ANOVA sex effect: $p=0.0757$, genotype effect:
1065 $p=0.1008$. **M)** Latency (s) to climb the platform during the visible phase of the MWM. Three-
1066 way ANOVA genotype effect: * $p=0.0220$; sex effect $p=0.1982$. **N, O)** Front- and hindlimb grip
1067 strength (gm) was tested three times and the average is shown. Two-way ANOVA sex
1068 effect: $p=0.1118$ (N) and $p=0.1924$ (O). **P)** Freezing behaviour was assessed during
1069 contextual fear conditioning training, when three shocks were administered. Three-way
1070 ANOVA sex effect: $p=0.07$, genotype effect: **** $p<0.0001$. **Q)** Freezing percentages in the
1071 context testing session, 24 h later. Two-way ANOVA sex effect: $p=0.1489$. **R)** Mean speed
1072 was higher in mutant mice, in line with their reduced freezing behaviour during training (two-
1073 way ANOVA genotype effect: ** $p=0.0053$). However, no differences were observed between
1074 genotypes during the 2-sec long foot shocks (Tukey's post hoc test $p=0.9943$ (shock 1),
1075 $p>0.9999$ (shock 2), $p=0.9998$ (shock 3), thus discarding differences in sensitivity and
1076 responses to shocks as a contributing factor. Data was analysed with two-way ANOVA (A,
1077 E, F) or repeated-measures two-way ANOVA (B, I, L, M, P, R) followed by Tukey's post-hoc
1078 test. Data in C, J, K, N, O and Q was analysed with Student's t-test, or Mann-Whitney test

1079 when appropriate. * $p < 0.05$, ** $p < 0.01$, *** $p < 0.001$, **** $p < 0.0001$. A one-sample t-test was
1080 used (K) to analyse whether time spent in the target quadrant was above chance. ## $p < 0.01$,
1081 ### $p < 0.001$, #### $p < 0.0001$. For all experiments, $n = 17$ +/+ male, $n = 14$ +/+ female, $n = 17$ Δ/Δ
1082 male and $n = 13$ Δ/Δ female mice. Female (squares) and male (diamonds) samples are
1083 included.

1084

1085 **Figure 4. Altered gene expression in *Kdm5b* ^{Δ/Δ} mice.**

1086 Hippocampi were dissected from naïve animals and RNAseq analyses were performed ($n = 4$
1087 animals/genotype). **A)** Heatmaps show differentially expressed genes in wildtype control
1088 (+/+) and mutant (Δ/Δ) mice. Yellow=upregulated and blue=downregulated in mutants. See
1089 Extended data Table 4-1 for detailed RNA-sequencing data information. **B)** Volcano plot
1090 displaying baseline gene expression changes between wild-type and *Kdm5b* ^{Δ/Δ} homozygous
1091 mutant mice. Red and blue dots depict differentially up- and downregulated genes,
1092 respectively. Differentially expressed immediate early genes are labelled. **C)** Immediate early
1093 gene expression in the dorsal hippocampus from WT and *Kdm5b* ^{Δ/Δ} mice was analysed by
1094 qPCR; $n = 9$ animals/genotype. Two-way ANOVA genotype effect *** $p = 0.0001$. **D)**
1095 Immunostaining of sections from DG and CA3 with an Npas4-specific antibody (magenta),
1096 counterstained with DAPI (grey) are shown. White arrowheads indicate positive nuclei. **E)**
1097 The number of Npas4-positive cells (arrowheads) was quantified in mm² areas of the CA3
1098 and DG. Scale bar, 200 μ m, 100 μ m for higher magnification images; $n = 10$ mice/genotype.
1099 Data is shown as mean \pm SEM, including both female and male mice. Data was analysed
1100 with Student's t-test (C, E): * $p < 0.05$, ** $p < 0.01$.

1101 **Figure 5. Learning-associated gene expression changes in *Kdm5b* ^{Δ/Δ} mice.**

1102 Wildtype (+/+) and *Kdm5b* ^{Δ/Δ} (Δ/Δ) mice were trained in the fear conditioning chamber and
1103 culled 1h or 3h later. Homecage, test-naïve mice were used as controls. Dorsal
1104 hippocampus was dissected and RNAseq analyses were performed. $n = 3$ males and 3

1105 females per genotype and timepoint. **A-D)** Differentially expressed genes were clustered by
1106 their expression trajectories with k means clustering (k=4). Selected genes within each
1107 cluster are shown on the right. **E-G)** Heatmaps show differentially expressed genes in
1108 control and mutant mice at baseline levels (E) or 1h (F) and 3h (G) after fear conditioning.
1109 Yellow = upregulated and blue=downregulated. **H,I)** Volcano plots display gene expression
1110 changes after conditioning. Red and blue dots depict differentially up- and downregulated
1111 genes, respectively, at 1h or 3h compared to control animals for each genotype.
1112 Differentially expressed activity-regulated genes are labelled in orange. Data is shown as
1113 mean \pm SEM, including female and male mice. Data was analysed with repeated measures
1114 two-way ANOVA (A-D): ***p<0.001, ****p<0.0001. See Fig. 5-1, Table 5-1 and Table 5-2 for
1115 extended data.

1116

1117 **Figure 6. *Kdm5b* knockdown in the dorsal hippocampus (CA1) of adult mice**
1118 **abrogates hippocampus-dependent memory consolidation and diminishes long-term**
1119 **potentiation.**

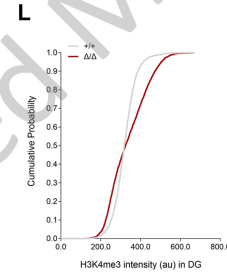
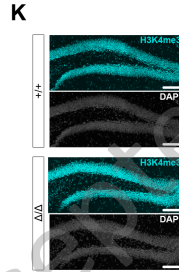
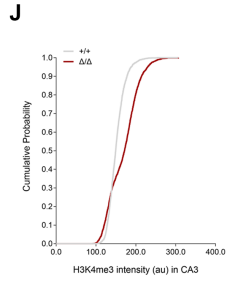
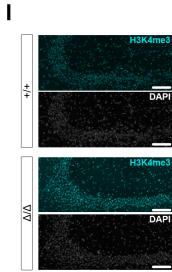
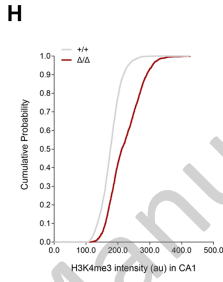
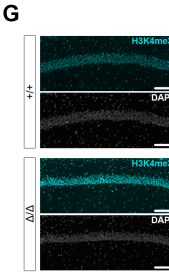
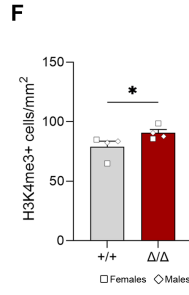
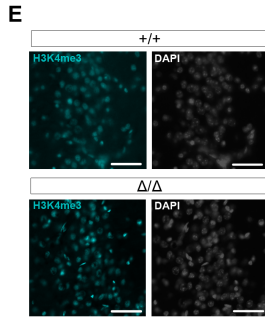
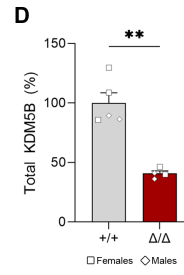
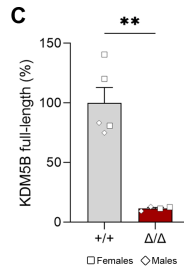
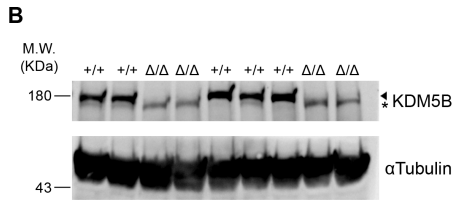
1120 **A)** Diagram of experimental work-flow. Approximately 3 weeks after stereotactic viral
1121 delivery into CA1, mice were habituated and tested in the object location memory task. Upon
1122 completion of behavioural tests, synaptic plasticity was assessed in acute brain slices from
1123 these mice. **B)** Representative immunostaining of dorsal hippocampus transduced with GFP-
1124 expressing AAV1, 11 days after surgery. Scale bar, 200 μ m. Panels display representative
1125 CA1, CA3 and DG inset images with GFP (green) and DAPI (blue) labelling. Scale bar,
1126 50 μ m. **C)** qRT-PCR analysis of *Kdm5b* expression, relative to *Hprt*, from total RNA extracted
1127 from the dorsal hippocampus at indicated times (3 and 7 weeks (wks) after viral delivery).
1128 N=3-5 mice/group. **D)** qRT-PCR analysis of *Kdm5b* and immediate early gene expression,
1129 relative to *Hprt*, from total RNA extracted from the dorsal hippocampus, 11 days post-
1130 transduction. Two-way ANOVA shRNA effect for IEGs: **p=0.0016. N=3 mice/group. **E)**
1131 Distance moved (cm) in the test arena (open field) on the first day of habituation as a

1132 measure of general activity (n=10 control and n=10 shRNA females). **F)** Discrimination index
1133 in the OLM task for control and shRNA mice during training and 24h long-term memory tests
1134 are shown. Note significant learning in control mice compared to training, but no significant
1135 learning in shRNA mice compared to controls (n=9 control and n=9 shRNA female mice).
1136 Two-way ANOVA interaction effect: *p=0.0257. **G)** Number of mice of each group (n=10
1137 each) showing spontaneous seizures during handling (pink), compared to no seizures (grey).
1138 Fisher's exact test: **p=0.0031. **H)** Short- and long-term plasticity changes measured from
1139 hippocampal area CA1b apical dendrites in acute hippocampal slices (n=8 slices from each
1140 group; n=4 mice/group). Following a 20 min stable baseline recording, theta burst stimulation
1141 (TBS, arrow) was delivered to induce LTP and recordings were followed for an additional 1h.
1142 The fEPSP slope measured from *Kdm5b* shRNA slices was noticeably lower relative to
1143 controls by the end of the recording period. Inset: representative traces collected during
1144 baseline (black line) and 60 min post-TBS (red line). Scale: 1 mV/5 ms. **I)** The mean
1145 potentiation 50-60 min post-TBS was significantly reduced in slices from *Kdm5b* shRNA
1146 mice relative to controls (**p = 0.0056, n=8 each). **J, K)** Short-term plasticity measures in
1147 slices from *Kdm5b* shRNA mice including (J) input/output curve and (K) paired-pulse
1148 facilitation did not reveal any significant differences from shScramble controls. Data is shown
1149 as mean \pm SEM, analysed with Student's T-test (C, D, E, I), two-way ANOVA (F) and Fisher's
1150 exact test (G). *p<0.05, **p<0.01, ***p<0.001. Control, shScramble; shRNA, shKdm5b.

1151

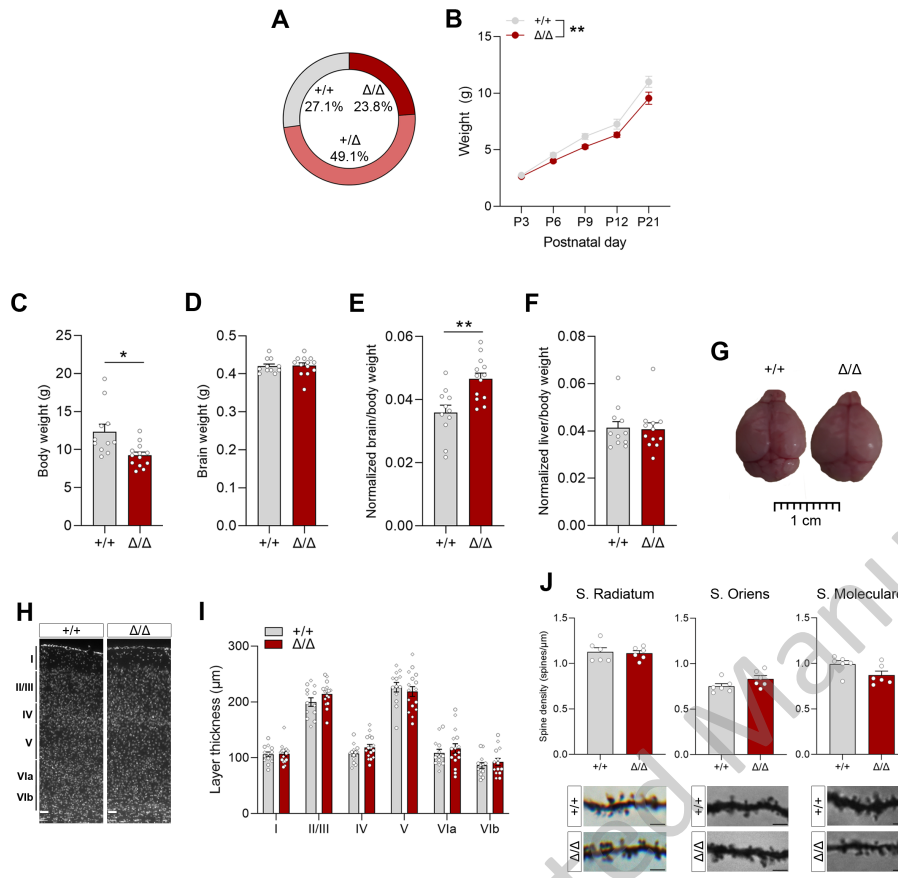
1152

1153



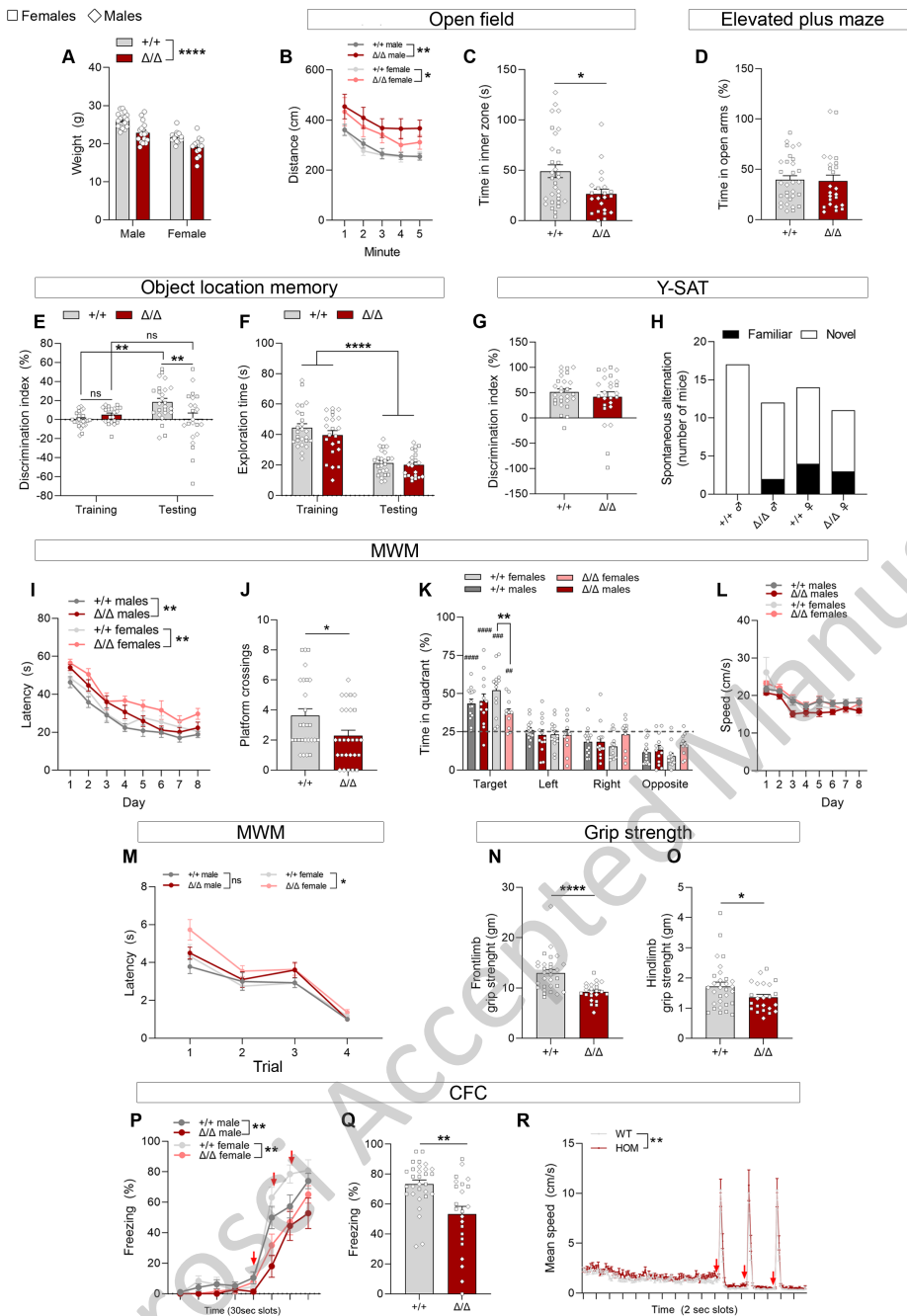
JNeurosci Acc

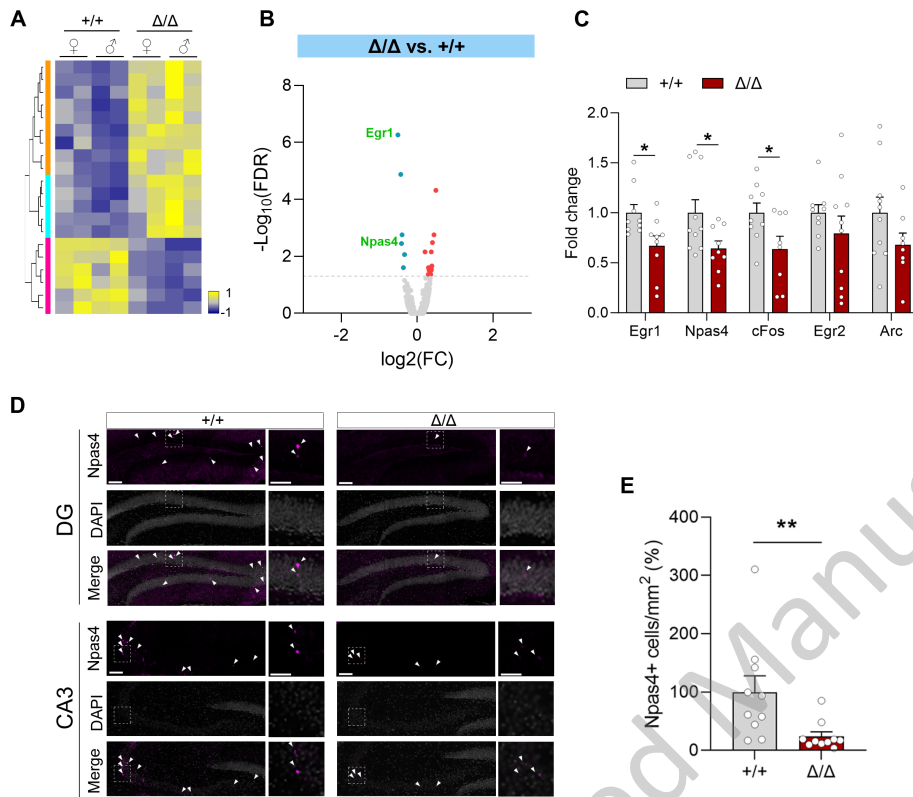
Manuscript



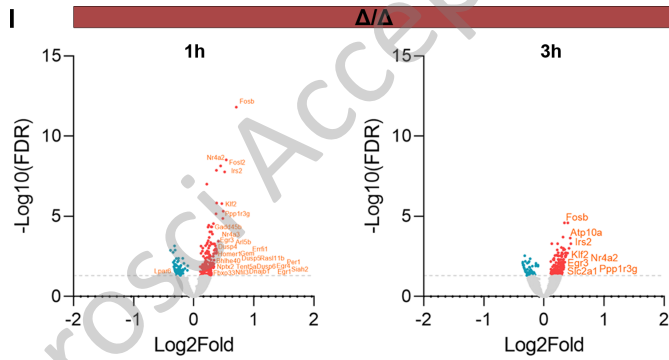
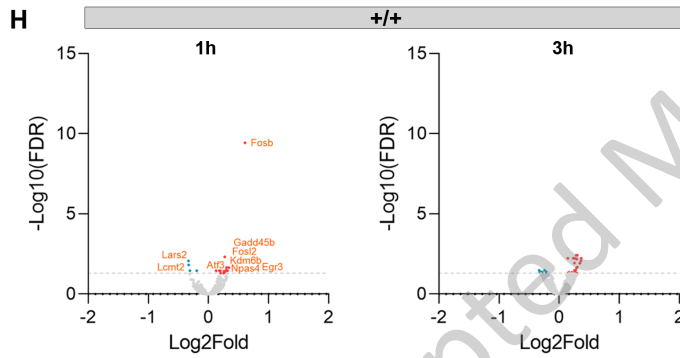
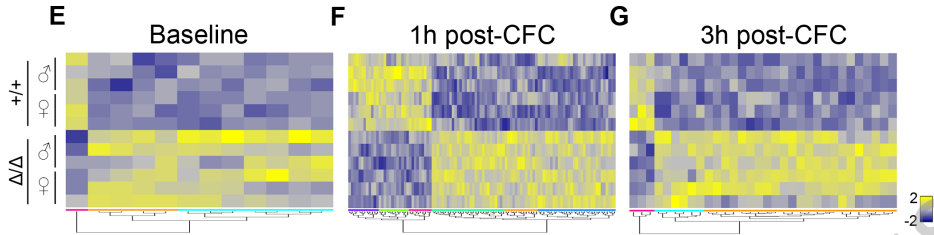
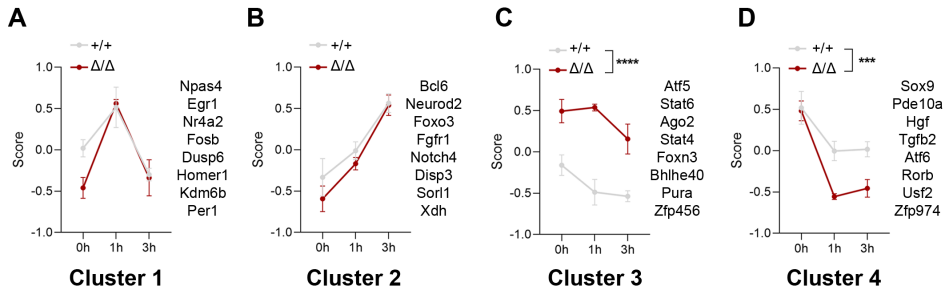
JNeurosci Accepted Manuscript

□ Females ◇ Males





JNeurosci Accepted Manuscript



JNeurosci Accepted Manuscript

